PTEN Regulates Myofibroblast Activation in Valvular Interstitial Cells based on Subcellular Localization

Dilara Batan[1,2,*], Georgios Tseropoulos[1,2,*], Bruce E. Kirkpatrick[1,2,3], Kaustav Bera[1,2], Alex Khang[1,2], Mary Weiser-Evans[4,5,6], Kristi S. Anseth[1,2]

[1] Department of Chemical and Biological Engineering, University of Colorado, Boulder, Colorado 80303, United States
2 The BioFrontiers Institute, University of Colorado, Boulder, Colorado 80303, United States
[3] Medical Scientist Training Program, School of Medicine, University of Colorado, Aurora, Colorado 80045, United States
[4] Department of Medicine, Division of Renal Diseases and Hypertension, University of Colorado, Anschutz Medical Campus, 12700 East 19th Avenue, C281, Research Complex 2, Room 7101, Aurora, Colorado 80045, USA.
[5] Center for Fibrosis Research and Translation, School of Medicine, University of Colorado, Anschutz Medical Campus, Aurora, Colorado 80045, USA.
[6] Department of Medicine, Cardiovascular Pulmonary Research Program, University of Colorado, Anschutz Medical Campus, Aurora, Colorado 80045, USA.

*Denotes equal contribution

Abstract

Aortic valve stenosis (AVS) is characterized by altered mechanics of the valve leaflets, which disrupts blood flow through the aorta and can cause left ventricle hypotrophy. These changes in the valve tissue result in activation of resident valvular interstitial cells (VICs) into myofibroblasts, which have increased levels of αSMA in their stress fibers. The persistence of VIC myofibroblast activation is a hallmark of AVS. In recent years, the tumor suppressor gene phosphatase and tensin homolog (PTEN) has emerged as an important player in the regulation of fibrosis in various tissues (e.g., lung, skin), which motivated us to investigate PTEN as a potential protective factor against matrix-induced myofibroblast activation in VICs. In aortic valve samples from humans, we found high levels of PTEN in healthy tissue and low levels of PTEN in diseased tissue. Then, using pharmacological inducers to treat VIC cultures, we observed PTEN overexpression prevented stiffness-induced myofibroblast activation, whereas genetic and pharmacological inhibition of

36 PTEN further activated myofibroblasts. We also observed increased nuclear PTEN localization in
37 VICs cultured on stiff matrices, and nuclear PTEN also correlated with smaller nuclei, altered
38 expression of histones and a quiescent fibroblast phenotype. Together, these results suggest that
39 PTEN not only suppresses VIC activation, but functions to promote quiescence, and could serve
40 as a potential pharmacological target for the treatment of AVS.

41 **Introduction**

42 Aortic Valve Stenosis (AVS) is a progressive cardiovascular disease that directly affects the
43 aortic valve leaflet matrix composition and mechanical properties, leading to disrupted blood flow
44 through the aorta[1] and eventual complications associated with left ventricular pressure-overload.[2]
45 When aortic valve leaflets thicken and stiffen as AVS progresses, significant deficiencies in
46 cardiac output result, which can lead to heart failure and death. AVS affects around 2% of the
47 population older than 65 with higher occurrences in males compared to females.[3] Symptomatic
48 AVS patients suffer high mortality rates if the condition is left untreated.[4] Currently, there are no
49 known effective pharmacological treatments for AVS, and surgical or transcatheter valve
50 replacement remains the standard of care for patients with severe disease. However, many patients
51 are ineligible for surgery, as valve replacement has many risks including valve leaks, bleeding,
52 and vessel damage.[1,5] As a result, a deeper molecular and mechanistic understanding of AVS is
53 necessary if one hopes to identify alternative pharmaceutical treatment strategies.

54 Valvular interstitial cells (VICs) are the main population of cells residing in aortic valve
55 leaflets, and these fibroblast cells are responsible for valve maintenance and repair following
56 injury. Because of their key role in valve homeostasis, VICs are highly sensitive to
57 physicochemical changes in the matrix microenvironment.[6–8] Specifically, VICs transition from
58 quiescent fibroblasts to activated myofibroblasts, characterized by formation of alpha-smooth

59 muscle actin (αSMA) stress fibers, increased proliferation, and elevated extracellular matrix
60 (ECM) deposition.[9] During fibrosis, the myofibroblast phenotype persists over time, leading to a
61 pathogenic accumulation of ECM , stiffening of the local microenvironment, and creating a
62 positive feedback loop that can accelerate disease progression.[10] Investigating
63 mechanotransduction pathways capable of reversing this process and restoring the quiescent
64 fibroblast phenotype continues to be a promising avenue for potential treatments.[11–15]

65 Hydrogels provide highly tunable microenvironments that can be adjusted to recapitulate the
66 stiffness of the valve matrix at different stages of fibrosis progression and enable researchers to
67 study VIC mechanosensing in a controlled manner.[16] In this work, the crosslinking density of
68 poly(ethylene glycol) (PEG) hydrogels was tailored to control the matrix mechanical properties,[17]
69 while the fibronectin-derived adhesive peptide, RDGS, was used to promote VIC-matrix
70 interactions.[18] When cultured on soft PEG hydrogels (~1-5 kPa), VICs maintained a quiescent
71 fibroblast phenotype, but transitioned to an activated myofibroblast phenotype on stiffer PEG
72 matrices (E'~13-30kPa).[15,19–22] Thus, these biomaterial systems provided a reliable *in vitro*
73 platform for VIC cultures in healthy and disease scenarios.

74 As valvular tissue stiffens during AVS progression, signaling through mechanosensitive
75 pathways can reveal essential signaling hubs governing cell phenotype and potentially serve as
76 druggable targets. Importantly, elevated levels of phospho-AKT (p-AKT), which indicates
77 increased activation of phosphoinositide 3-kinase (PI3K)/AKT pathway, have been observed in
78 the fibroblast to myofibroblast transition (FMT).[23] In this regard, the pathway has been presented
79 as a master regulator of idiopathic pulmonary fibrosis.[23] Similarly, we have previously
80 demonstrated that PI3K/AKT signaling is increased on stiff substrates and is necessary for

81 substrate stiffness induced myofibroblast activation in VICs.[11,24] These findings suggest that
82 targeting the PI3K/AKT pathway may be a promising approach for treating fibrotic diseases.

83 Phosphatase and tensin homolog (PTEN), which is a negative regulator of the PI3K/AKT
84 pathway, has been proposed as a potential target for therapeutic intervention in fibrotic disease.[25–
85 27] For example, Lu *et al.* demonstrated that overexpression of PTEN in the mouse model
86 superPTEN protects against angiotensin II induced vascular fibrosis.[26] Further, the same group
87 later observed that small molecule drugs, such a 5-azacytidine and itraconazole, increase PTEN
88 levels and are able to ameliorate effects of increased signaling through the PI3K/AKT pathway.[26,28]
89 Complementary to the overexpression studies, Parapuram *et al*. demonstrated that loss of PTEN
90 leads to overproduction of collagen and is enough to induce fibrosis in lung and skin tissues.[27,29]
91 Similar studies were conducted in mammary gland tissue by Jones *et al.* and further confirmed that
92 PTEN regulates extracellular matrix deposition and collagen organization, steps that are essential
93 in fibrosis development.[30] Collectively, these findings suggest that targeting the PI3K/AKT
94 through PTEN may hold promise for developing novel therapies for fibrotic diseases. However,
95 no previous work has been conducted specifically investigating the effects of PTEN in the context
96 of AVS. Motivated by this, we aimed to explore the role of PTEN in VIC myofibroblast activation
97 and its potential as a therapeutic target for aortic valve disease.

98 Results herein reveal a major role of PTEN in regulating VIC fibroblast and myofibroblast
99 phenotypes. Initially, we observe a loss of PTEN protein in diseased human valve leaflet sections
100 compared to healthy ones. To test the specific role of mechanotransduction on PTEN expression
101 and VIC phenotype, we tailored the modulus/stiffness of PEG hydrogels to direct VICs towards
102 either a fibroblast (E' ~3 kPa) or a myofibroblast (E' ~13.4 kPa) majority population. Next, we
103 demonstrate that pharmacologically increased PTEN levels promote a more quiescent phenotype

104 for VICs cultured on stiff hydrogels, while chemical and genetic inhibition of PTEN increased
105 myofibroblast activation on soft hydrogels. Interestingly, the minority fibroblast population on
106 stiff matrices had higher nuclear localization of PTEN compared to the majority myofibroblast
107 population. In addition, the population of cells with high PTEN nuclear localization correlated
108 with smaller nuclei and VIC quiescence. The regulation of VIC activation by PTEN was further
109 verified by shRNA knockdown, as well as overexpression (nuclear localization and exclusion
110 signal tagged) experiments *in vitro*. Our results led us to hypothesize that nuclear PTEN may play
111 an additional role, beyond cytoplasmic regulation of PI3K/AKT, maintaining VIC quiescence by
112 regulating histone expression on stiff matrices. Overall, in this study we show that PTEN is a major
113 regulator of VIC fibroblast to myofibroblast transition and can serve as a future target for
114 pharmaceutical interventions.
115

116 **Materials and Methods**

117
118 *Hydrogel precursor synthesis*

119 Poly(ethylene glycol) photodegradable diacrylate PEGdiPDA (MW approximately 3400 Da) was
120 synthesized and characterized according to a previous method.[31] >90% acrylate functionalization
121 was verified by ^{1}H NMR. The adhesive peptide, acrylamide diethylene glycol-diethylene glycol-
122 glycine-arginine-glycine-aspartic acid-serine-glycine (Ac-OOGRGDSG), was synthesized via 9-
123 fluorenylmethyloxycarbonyl (Fmoc)/1-[bis(dimethylamino)methylene]-1H-1,2,3-triazolo[4,5-b]
124 pyridinium 3-oxid hexafluorophosphate (HATU) coupling strategy on Rink Amide
125 methylbenzhydryl amine (MBHA) resin (0.500 mmol) using a Protein Technologies Tribute
126 automated solid-phase peptide synthesis machine and characterized using electrospray ionization
127 (ESI) mass spectroscopy.[31]

128

129 *Formation of hydrogels*

130 The preparation of photo-softening PEGdiPDA hydrogels was adapted from previously described
131 protocols.[31] PEGdiPDA was co-polymerized with poly(ethylene glycol) monoacrylate (PEGA;
132 Mn~400 Da; Monomer-Polymer and Dajac Laboratories) and acryl-OOGRGDSG in PBS via
133 redox-initiated free radical polymerization. Gel solutions were prepared with 7.0 wt% PEGdiPDA,
134 6.8 wt% PEGA, 5 mM acryl-OOGRGDSG, 0.2 M ammonium persulfate (APS) and 0.1 M
135 tetramethylethylenediamine (TEMED). Gels were formed on acrylated cover glass after the
136 addition of APS/TEMED, with diameters of 12, 15, or 25 mm and a thickness of 100 μm. Gels
137 were allowed to cure for 6 min and washed and stored in PBS before cell seeding. Soft hydrogels
138 were prepared by irradiating the initial hydrogels with UV light (λ = 365 nm; I_0 = 10 mW/cm^2) for
139 6 minutes.

140

141 *Swollen rheological characterization*

142 Optically thin PEGdiPDA hydrogels (thickness = 200 μm) were made between two sigmacoted
143 glass slides separated with a spacer using the formulations above and allowed to swell in PBS
144 overnight. A rheometer (TA Instruments DH-R3) with a parallel plate accessory was used to
145 measure the shear modulus of the PEGdiPDA hydrogel before and after photo-degradation. The
146 equilibrium storage modulus (G′) was measured using a dynamic time sweep (γ = 1%; ω = 1 rad/s),
147 as determined to be in the linear regime for this material. For *in situ* degradation, a quartz plate
148 was used, and the rheometer was equipped with a 365 nm light source (λ = 365 nm; I_0 = 10
149 mW/cm^2; Omnicure 1000, LumenDynamics). After network formation, the hydrogel was exposed
150 to 365 nm light for 6 minutes, and the change in G' was monitored using the same dynamic time

151 sweep parameters. The same dynamic time sweep measurements were used to obtain final G' as a
152 function of light exposure time. G' was measured and converted to Young's modulus (E) using a
153 Poisson's ratio of 0.5.[32]

154 *Valvular Interstitial Cell (VIC) isolation and culture*

155 Primary VICs were isolated from aortic valve leaflets from fresh male porcine hearts (Hormel) as
156 previously described.[14,20,21,24]. Briefly, aortic valve leaflets were excised from the hearts and rinsed
157 in Earle's Balanced Salt Solution (EBSS, Life Technologies) supplemented with 50 U/mL
158 penicillin and 50 µg/mL streptomycin (Thermo Fisher), and 1 µg/mL amphotericin B (Thermo
159 Fisher). Leaflets were incubated in a 250 U/mL type II collagenase (Worthington) solution in
160 EBSS for 30 min under 5% CO2 at 37˚C with gentle shaking. Valvular endothelial cells were
161 removed by vortexing leaflets at maximum speed for 30 seconds. Leaflets were transferred to fresh
162 collagenase solution and incubated for 60 min under 5% CO2 at 37˚C with gentle shaking. Leaflets
163 were vortexed again for 2 minutes to dislodge valvular interstitial cells (VICs), and the entire
164 solution was passed through a 100 µm cell strainer. The strained cell solution was centrifuged at
165 0.2g x 20 minutes. Pelleted cells were resuspended in VIC expansion media compromising of
166 M199 media (Life Technologies) 15% fetal bovine serum (FBS, Life Technologies), 50 U/mL
167 penicillin, 50 µg/mL streptomycin (Thermo Fisher), and 1µg/mL amphotericin B (Thermo Fisher).
168 Cells were cultured in T-75 flasks for expansion until 80% confluency was obtained. Cells were
169 harvested using trypsin (Life Technologies) to be frozen in 50% fetal bovine serum (FBS) (Life
170 Technologies), 45% M199 media (Life Technologies), and 5% DMSO (Sigma-Aldrich).

171 For experimental use, cells were thawed and cultured in T-75 flasks in 15% FBS
172 supplemented M199 media until 80% confluent. Cells were counted after harvesting using an
173 automated hemocytometer (Countess). A seeding density of 15,000 cells/cm^2 was used for VICs

174 on hydrogels, with growth media consisting of M199 media supplemented with 1% FBS,
175 penicillin-streptomycin, and fungizone. 12 mm hydrogels were used for immunostaining
176 experiments; 25 mm hydrogels were used for real-time quantitative polymerase chain reaction
177 (RT-qPCR) to increase the measurable RNA content.
178
179 *Hydrogel Immunostaining*
180 VICs were fixed in 4% paraformaldehyde (PFA, Electron Microscopy Sciences) in PBS for 20
181 minutes and rinsed twice with PBS. Cells were permeabilized with 0.1% TritonX-100 (Fisher
182 Scientific) in PBS for 20 minutes followed by 1 hour of blocking in 5% bovine serum albumin
183 (BSA, Sigma-Aldrich). Primary antibodies were diluted in 5% BSA and incubated at 4˚C overnight
184 at given concentrations: α-smooth muscle actin (αSMA, mouse, Cat. No. ab7817, Abcam) at 1:300
185 dilution, PTEN (rabbit, Cat. No. D8H1X, Cell Signaling) at 1:300 dilution. Primary antibody was
186 washed off the cells twice with PBST (0.5% Tween-20 in PBS), and once in PBS. Samples were
187 incubated in secondary antibody solution of 1:200 dilution goat anti-mouse Alexa 488 (Life
188 Technologies), 1:500 dilution of goat anti-rabbit Alexa 648 (Life Technologies), 1:5000 dilution
189 of HCS Cell Mask (Life Technologies), and 1:1000 dilution of DAPI (Life Technologies) for 1
190 hour before rinsing twice with PBST (0.005% Tween-20 in PBS) and once in PBS. For imaging,
191 hydrogels were inverted onto a glass-bottom 24-well plate (Cellvis) and visualized using an
192 Operetta high-content confocal microscope using a 20x air objective (Perkin Elmer).
193 Immunofluorescence intensity in immunostained cells was quantified using Harmony software
194 (Perkin Elmer). PTEN nuclear localization was quantified by dividing PTEN average nuclear
195 signal by PTEN average cytoplasmic signal.
196

197 *Isolation of mRNA and Real-Time Quantitative Polymerase Chain Reaction (RT-qPCR)*

198 RNA was isolated according to manufacturer's instructions using an RNeasy Micro Kit (Qiagen).
199 RNA concentration was quantified using ND-1000 NanoDrop Spectrophotometer (Thermo
200 Fischer). cDNA was produced using iScript Reverse Transcription Supermix kit (Bio-Rad) on a
201 Mastercycler (Eppendorf). Relative mRNA levels were measured with SYBR Green reagents on
202 an iCycler (Bio-Rad). Results were normalized to the housekeeping gene RPL30 (Ribosomal
203 protein L30). Custom primers are presented in **Table S1**.

204

205 *PTEN lentiviral knockdown*

206 Two shRNA sequences were purchased from Millipore Sigma and cloned into the pLKO.1
207 lentiviral vector. Virus was produced utilizing second generation packaging plasmids PSPAX2
208 and pnd2.g as described previously.[33] Briefly, HEK 293T cells were transfected with the packaging
209 plasmids and shRNA for PTEN and two viral batches were collected after 24 and 48 hours. P1
210 VICs were transduced with the viral constructs for 3 hours, and VICs that incorporated the virus
211 were selected with puromycin (1ug/ml) for 3 days. The genetically modified VICs were allowed
212 to proliferate on TCPS until 80% confluence and subsequently passaged on soft or stiff hydrogels
213 (E' ~3 kPa, E' ~13.4 kPa, respectively). The potency of shRNA PTEN knockdown was validated
214 though immunohistochemistry for PTEN staining and qPCR testing for PTEN mRNA, and the
215 most potent knockdown sequence was selected for experiments reported herein.

216

217 *Transfection with NES and NLS plasmid constructs*

218 VICs were seeded on stiff hydrogels at a density of 6000 cells / cm^2 and incubated overnight.
219 Transfection media was prepared the next day using lipofectamine 3000 at a dilution of 0.5ul in
220 50ul of Opti-MEM reduced serum media per well and vortexed. The plasmids (Addgene PTEN

221 NES Plasmid# 10932, Addgene PTEN NLS Plasmid# 10933) were amplified using the Qiagen^{TN}
222 mini prep kit and diluted in a concentration of 1ug/ul. The control condition consisted of
223 lipofectamine and Opti-MEM only. The growth media was removed from wells and transfection
224 media was added. The transfection plate was incubated for 1 hour and then washed three times
225 with Opti-MEM. Subsequently, growth media was added and the plate was incubated for 3 days,
226 after which the plate was fixed and prepared for immunohistochemical characterization.
227

228 *Heart valve tissue histology*

229 Samples of aortic healthy and diseased (AVS) valve leaflets were acquired from deceased or heart
230 transplant patients at the University of Colorado Anschutz Medical Campus **(Table S2)**. Tissues
231 were fixed in 4% paraformaldehyde for 10 minutes and embedded in Tissue Tek O.C.T. for
232 subsequent cryosectioning. The sections were washed 3 times with PBS and permeabilized with
233 0.1% TritonX for 1 hour and blocked with 5% goat serum, 5% BSA, and 0.01% TritonX for 1
234 hour. The sections were treated with the following primary antibodies (αSMA, mouse, Cat. No.
235 ab7817, Abcam at 1:300 dilution, PTEN rabbit, Cat. No. D8H1X, Cell Signaling at 1:300 dilution)
236 sequentially over 2 days with 2 overnight incubations with the primary antibody in blocking buffer
237 (dilution 1:200) and 1 hour incubation with secondary antibody (1:400). The tissues were imaged
238 on an Nikon A1R confocal microscope and analyzed using ImageJ.
239

240 *Statistical Analysis*
241
242 Data are presented as mean ± standard deviation with a minimum of three biological and four
243 technical replicates for all studies unless otherwise stated. Outliers were removed using Robust
244 Outlier (ROUT) method (set at 1%). Significance was defined as *P<0.05, **P<0.01, ***P<0.005,

245 ****P<0.001 using a t-test for comparison of two samples and one-way analysis of variance
246 (ANOVA) for comparison of three or more samples. Statistics were performed in GraphPad Prism.
247

248 **Results**

249 *PTEN levels are lower in diseased human valve leaflets compared to healthy valves*

250 As previous studies have demonstrated that loss of PTEN is involved in fibrosis development, we
251 wanted to test whether PTEN levels were changed with AVS development. To do this, we
252 immunostained human valve leaflet tissue sections from healthy and diseased patients for DAPI,
253 αSMA, and PTEN and performed histological analysis targeted towards the levels of αSMA and
254 PTEN. In healthy tissue, we observed high levels of PTEN and low levels of αSMA (**Figure 1 A-**
255 **C**). In diseased tissue, significantly higher levels of αSMA and minimal levels of PTEN were
256 observed, indicating an inverse correlation, and implicating a protective role for PTEN against
257 fibrosis development in valve leaflets (**Figure 1 A**). These results motivated us to investigate the
258 role of PTEN in VIC activation *in vitro,* building on previous work that utilizes soft and stiff
259 hydrogels to recapitulate VIC myofibroblast differentiation and differential expression of αSMA,
260 dependent on substrate stiffness.

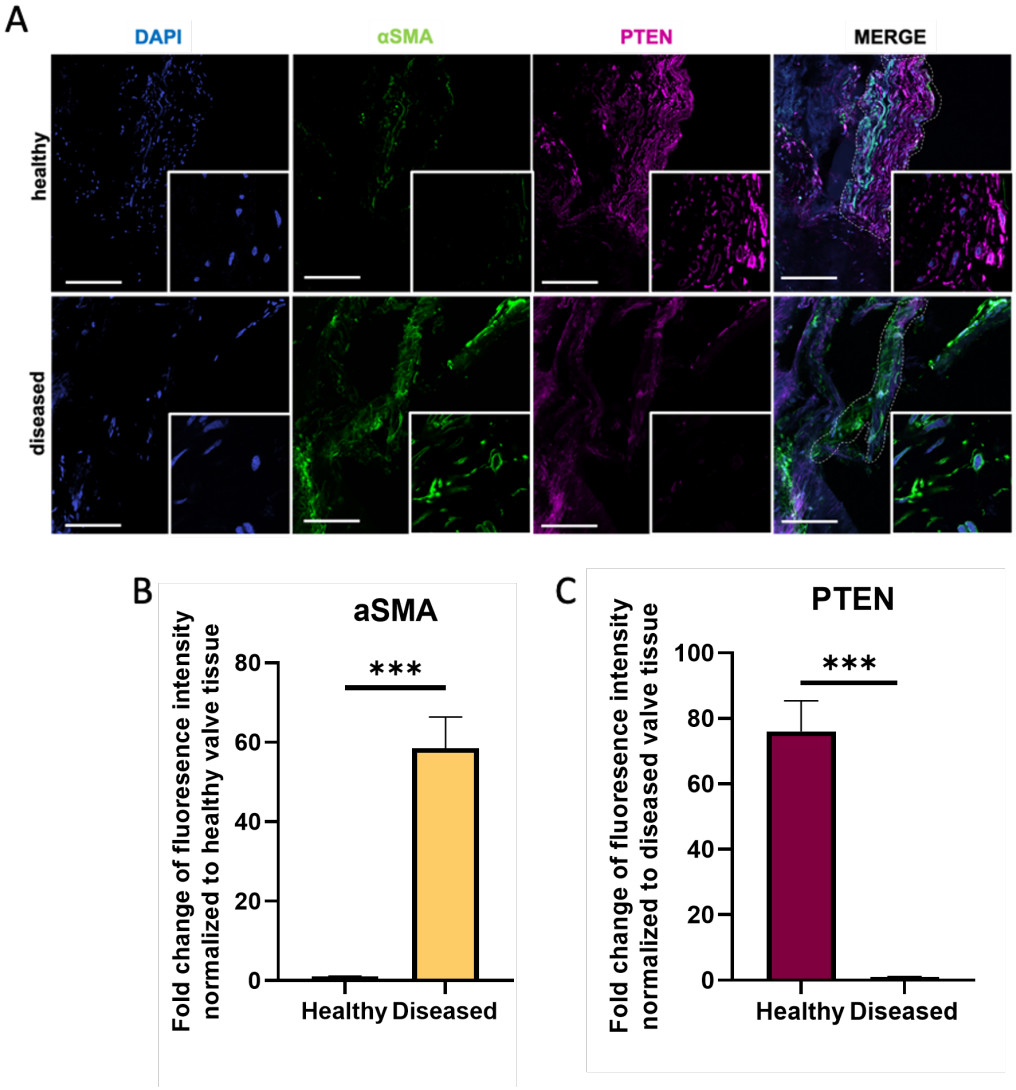

<u>Figure 1:</u> PTEN and αSMA levels inversely correlate in healthy and AVS human aortic valve tissue. A. Representative histological images of AVS and healthy human aortic valve tissue (male) stained for DAPI (blue), PTEN (magenta) and αSMA (green) levels in valvular interstitial cells. Scale bar = 50 µm **B.** Quantification of average αSMA intensity (normalized to DAPI per mm^2) for healthy and diseased tissue within the marked area in A. (normalized to DAPI per mm^2, n=5 fields of view per tissue, t-test, ***$p<0.001$). C. Quantification of PTEN intensity (normalized per mm^2) for healthy and diseased tissue within the marked area. (n=5 fields of view per tissue, t-test, ***$p<0.001$)

277 *PTEN levels inversely correlate with αSMA levels in VIC hydrogel cultures*
278
279 Motivated by the results from human valve samples, we wanted to test the effect of substrate
280 stiffness on PTEN expression levels. To do this, we initially cultured VICs on soft and stiff
281 hydrogels to identify conditions which promote a majority fibroblast phenotype on soft hydrogels
282 and a majority myofibroblast phenotype on stiff hydrogels. We synthesized PEG-acrylate
283 hydrogels supplemented with a fibronectin-derived peptide sequence, arginine-glycine-aspartic
284 acid-serine (RGDS) to allow for cell adhesion and facilitation of cell-matrix interactions. We
285 formulated soft (Young's modulus (E') = ~2.8 kPa) and stiff hydrogels (Young's modulus
286 (E') = ~13.4 kPa) to match the modulus of healthy and diseased valve leaflet tissue to mimic the
287 local microenvironmental VIC mechanosensing in AVS **(Supplementary Figure 1)**. Consistent
288 with previous data, we observed a quiescent fibroblast VIC phenotype on soft hydrogels and an
289 activated myofibroblast phenotype on stiff gels, as identified by the presence and intensity of
290 αSMA **(Figure 2 A,B)**. In addition to the αSMA protein produced, the VIC morphology cultured
291 on soft hydrogels was significantly smaller in cell and nuclear area compared to VICs cultured on
292 stiff hydrogels **(Supplementary Figure 1 B-C)**. Next, to determine if PTEN plays a protective
293 role against VIC myofibroblast activation, we examined protein levels in VICs cultured on the
294 same soft and stiff hydrogels. We observed that VICs displayed significantly higher PTEN levels
295 when cultured on soft hydrogels compared to stiff hydrogels, inversely correlating with αSMA
296 levels and myofibroblast activation **(Figure 2 C,D)**.

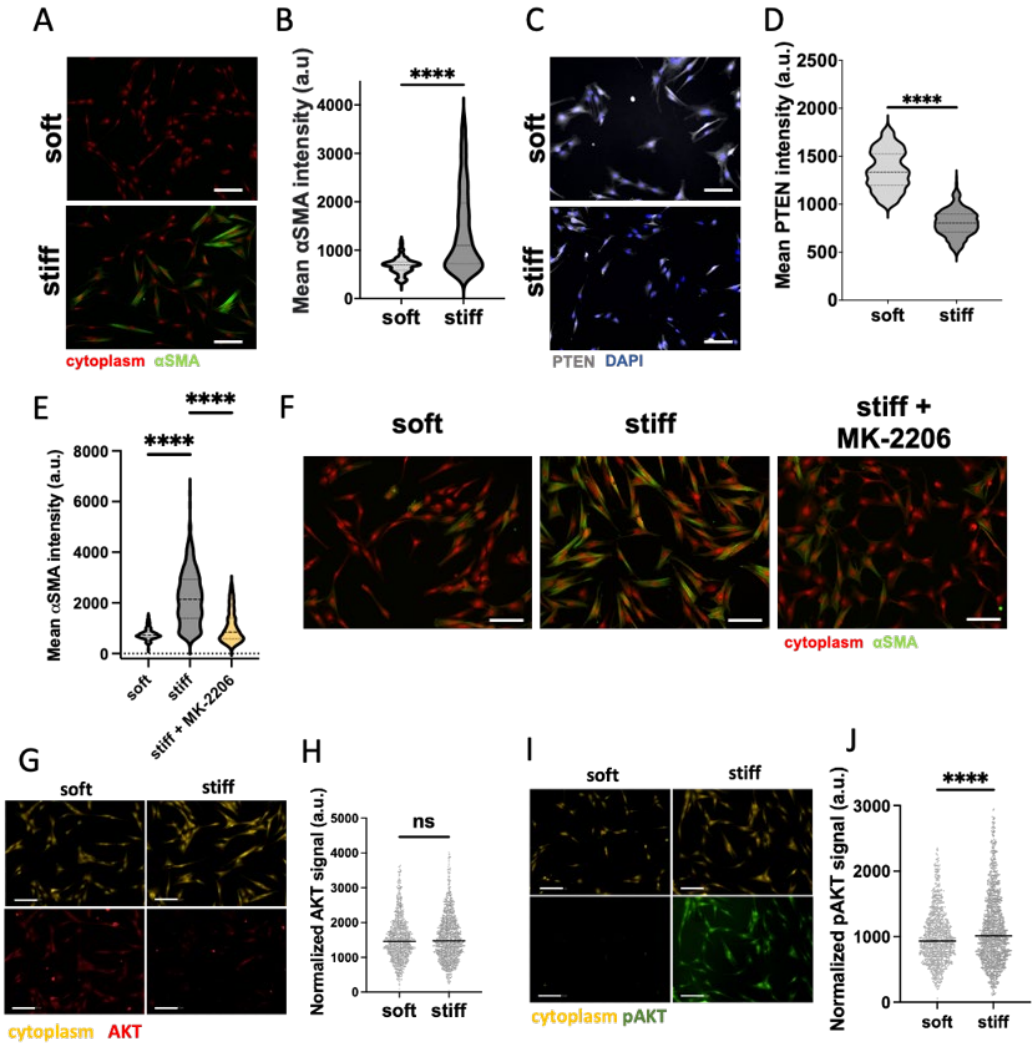

<u>Figure 2:</u> PTEN levels inversely correlate with myofibroblast activation in VICs A. Representative images of VICs cultured on soft and stiff hydrogels for 3 days, αSMA (green) and cytoplasm (red). Scale bar = 100 µm **B.** Quantification of αSMA (green) intensity for A. (n>750 cells from 4 hydrogels, unpaired t test, ****p<0.001). **C.** Representative images of PTEN (gray) levels in VICs cultured on soft and stiff hydrogels for 3 days. **D.** Quantification of PTEN intensity for C. (n>440 cells from 3 hydrogels, unpaired t test, ****p<0.001). **E.** Quantification of αSMA (green) intensity for F. **F.** Representative images of VICs cultured on soft and stiff hydrogels for 3 days treated with DMSO vehicle or 5 µM AKT inhibitor MK-2206, αSMA (green) and cytoplasm(red). Scale bar = 100 µm (n>750 cells from 4 hydrogels, unpaired t test, ****p<0.001). **G.** Representative images of VICs cultured on soft and stiff hydrogels for 3 days, AKT (red) and cytoplasm (yellow). Scale bar = 100 µm **H.** Quantification of AKT (red) intensity for G. (n>920 cells from 3 hydrogels, unpaired t test). **I.** Representative images of VICs cultured on soft and stiff hydrogels for 3 days, pAKT (green) and cytoplasm (yellow). Scale bar = 100 µm **J.** Quantification of pAKT (green) intensity for I. (n>1000 cells from 3 hydrogels, unpaired t test, ****p<0.001).

315

316 Since PTEN is a known inhibitor of the PI3K/AKT pathway, we sought to verify its potential
317 role in influencing stiffness-induced PI3K/AKT activity in VICs myofibroblast cultured on soft
318 and stiff hydrogels. Specifically, we used a highly specific and widely used small molecule AKT
319 inhibitor, MK-2206, and introduced it to activated VICs cultured on stiff hydrogels.[34–36] We found
320 that treatment with 5μM MK-2206 significantly reduced VIC αSMA expression when cultured on
321 stiff hydrogels compared to untreated controls, and promoted a quiescent fibroblast population
322 **(Figure 2 E,F, Supplementary Figure 2)**. Further, we observed similar levels of AKT in VICs
323 cultured on soft and stiff hydrogels; however, pAKT levels were significantly higher in VICs
324 cultured on stiff hydrogels (**Figure 2 G-J**). This observation supports the notion that PI3K/AKT
325 is a key mechanoregulator of VIC myofibroblast activation in stiff microenvironments.[24]

326

327 *PTEN activators decrease VIC activation in stiff hydrogel microenvironments*

328 Next, we wanted to investigate if increasing PTEN levels in VICs cultured on stiff hydrogels
329 would play a protective role against myofibroblast activation. To test this, we used two small
330 molecule PTEN activators that have been shown to increase cellular PTEN levels.[28,37] Initially, we
331 treated VICs cultured on TCPS with varying doses of the PTEN activators, 5-azacytidine or
332 itraconazole, and compared these to the DMSO vehicle control. We tested PTEN mRNA levels
333 using a concentration range (100 nm, 1 μM, and 10 μM) of 5-azacytidine and itraconazole and
334 observed that PTEN levels were significantly increased with 10 μM treatment of both 5-
335 azacytidine (**Figure 3A**) and itraconazole (**Supplementary Figure 3**).

336

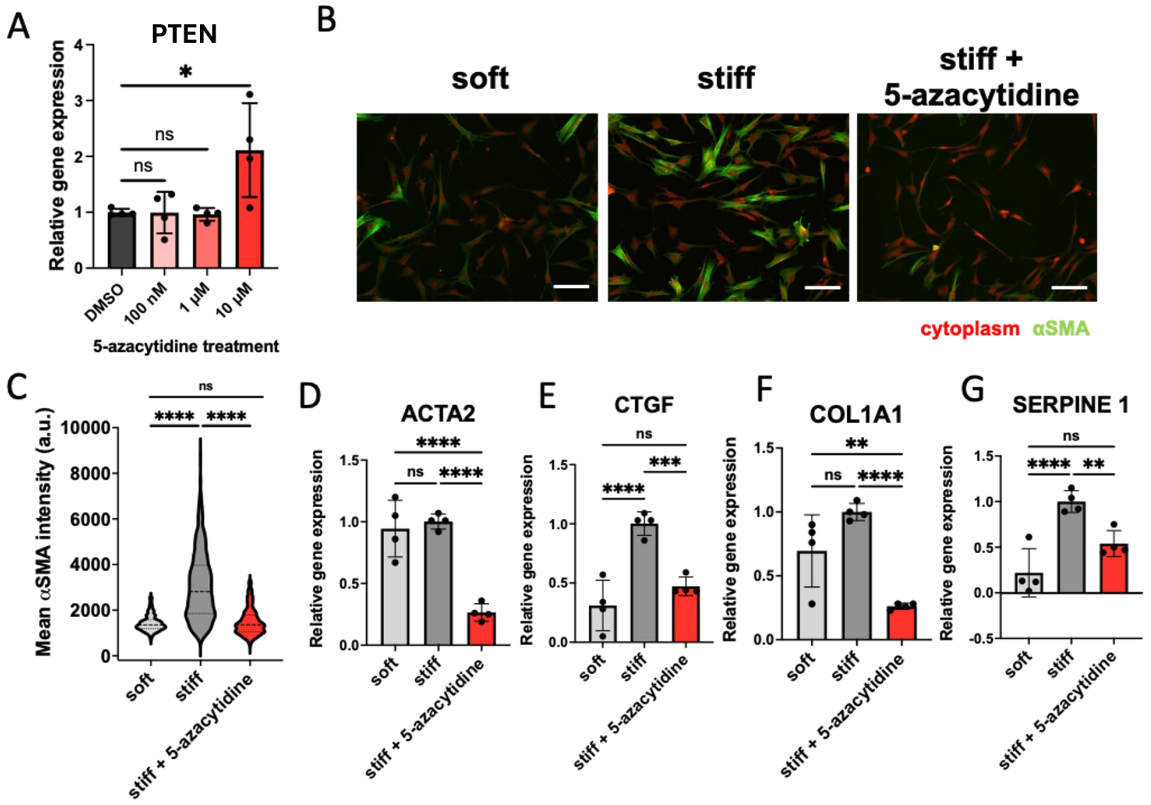

<u>Figure 3:</u> PTEN activators decrease myofibroblast activation in VICs A. Relative mRNA expression levels of PTEN in VICs cultured on TCPS with treatment of vehicle or increasing concentration of the PTEN activator, 5-azacytidine, n=4 wells, means ± SD shown, one-way ANOVA test, *p < .05 ,**p < .01. **B.** Representative images of VICs cultured on soft and stiff hydrogels for 3 days in the presence of vehicle or PTEN activator 5-azacytidine, αSMA (green) and cytoplasm (red). Scale bar = 100 µm. **C.** Quantification of αSMA intensity for B (n>600 cells from 4 hydrogels, one-way ANOVA test, ****p<0.001). **D-G.** Relative mRNA expression levels of fibrotic genes in VICs cultured on soft or stiff hydrogels treated with vehicle or PTEN activator 5-azacytidine for 3 days, n=4 hydrogels, one-way ANOVA test, *p < .05 ,**p < .01, ***p < .001,****p<0.001.

After verifying that PTEN levels could be elevated using small molecule activators, we treated VICs cultured on stiff hydrogels with either vehicle or 5-azacytidine and itraconazole with previously determined concentrations **(Supplementary Figure 4 A-D)**. We observed that VICs treated with PTEN activators displayed significantly lower levels of αSMA compared to the vehicle treated stiff hydrogel culture controls at levels resembling the soft hydrogel negative controls **(Figure 3 B,C, Supplementary Figure 5 A,B)**. In addition to having lower levels of

355 αSMA, VICs treated with PTEN activators also displayed a significantly smaller cell size and
356 nuclear area when compared to DMSO treated controls **(Supplementary Figure 6 A,B)**.
357 To more broadly assess the role of PTEN in myofibroblast activation, VICs were cultured
358 in the presence of PTEN activators or DMSO vehicle, and qPCR was performed to determine the
359 relative expression of myofibroblast associated genes, namely alpha-Smooth Muscle Actin
360 (ACTA2), Connective Tissue Growth Factor (CTGF), Serpin Peptidase Inhibitor clade E member
361 1 (SERPINE1), and Collagen type 1A1 (COL1A1). The expression of all four genes was
362 significantly decreased in VICs cultured on stiff hydrogels treated with PTEN activators compared
363 to the vehicle controls at levels resembling the soft hydrogel negative control conditions **(Figure**
364 **3 D-G, Supplementary Figure 5 C,D)**. These results suggest that PTEN influences multiple
365 markers of VIC myofibroblasts and that the effects are observable after 72 hours of treatment.
366
367 *Chemical and genetic PTEN inhibition increases VIC myofibroblast activation in soft hydrogel*
368 *microenvironments*
369 To further validate the role of PTEN in myofibroblast activation, we next performed a series
370 of studies inhibiting PTEN activity by introducing chemical and genetic perturbations. Initially we
371 tested the effects of a potent PTEN phosphatase inhibitor bpV(HOpic) on VIC myofibroblast
372 activation, as measured by αSMA expression.[38] Quiescent VICs cultured on soft hydrogels treated
373 with 100 nM of bpV(HOpic) displayed significantly higher levels of αSMA protein compared to
374 cells treated with the DMSO control **(Figure 4 A,B)**. In addition to αSMA protein content, ACTA2
375 gene expression levels were also elevated with PTEN inhibitor treatment **(Figure 4 C)**. These
376 results suggest that inhibition of PTEN phosphatase activity alone can promote myofibroblast
377 activation in VICs. However, interestingly, we observed non-significant changes in mRNA levels

378 of COL1A1 and SERPINE 1, suggesting more than just phosphatase activity of PTEN is important
379 to induce these transcriptional changes (**Supplementary Figure 7**).
380 In addition to chemical PTEN inhibition, we utilized lentiviral shRNA knockdowns of PTEN
381 in transduced early passage VICs. PTEN protein levels in the knockdown VICs were significantly
382 reduced compared to the scrambled shRNA controls on both soft and stiff hydrogels. **(Figure 4**
383 **D,F, Supplementary Figure 8 A,C)**. We cultured scrambled or PTEN knockdown VICs on both
384 soft and stiff hydrogels. On soft hydrogels, consistent with our previous data, we observed
385 enhanced PTEN expression and low levels of VIC myofibroblast activation (**Figure 4 D**), but
386 PTEN knockdown on soft hydrogels resulted in increased levels of αSMA **(Figure 4 E,F)**. On stiff
387 hydrogels, we observed lowered levels of PTEN with higher levels of αSMA (**Supplementary**
388 **Figure 8 A-C**). However, the effect of PTEN on VICs cultured on stiff hydrogels was much lower
389 compared to soft hydrogel conditions, as VICs are already activated on stiff hydrogels, but the
390 effects observed were statistically significant **(Supplementary Figure 8 B,C)**. After confirming
391 that PTEN protein levels were lower with our shRNA constructs, we next quantified mRNA
392 expression levels of known fibrotic genes **(Figure 4 G)**. Compared to scrambled shRNA controls,
393 PTEN knockdown VICs displayed higher levels of ACTA2, and COL1A1 expression.
394 Collectively, these results further validate PTEN's role as a regulator of the fibroblast-to-
395 myofibroblast transition in VICs, using hydrogels as a mechano-regulator to introduce quiescence
396 or activating matrix signals.

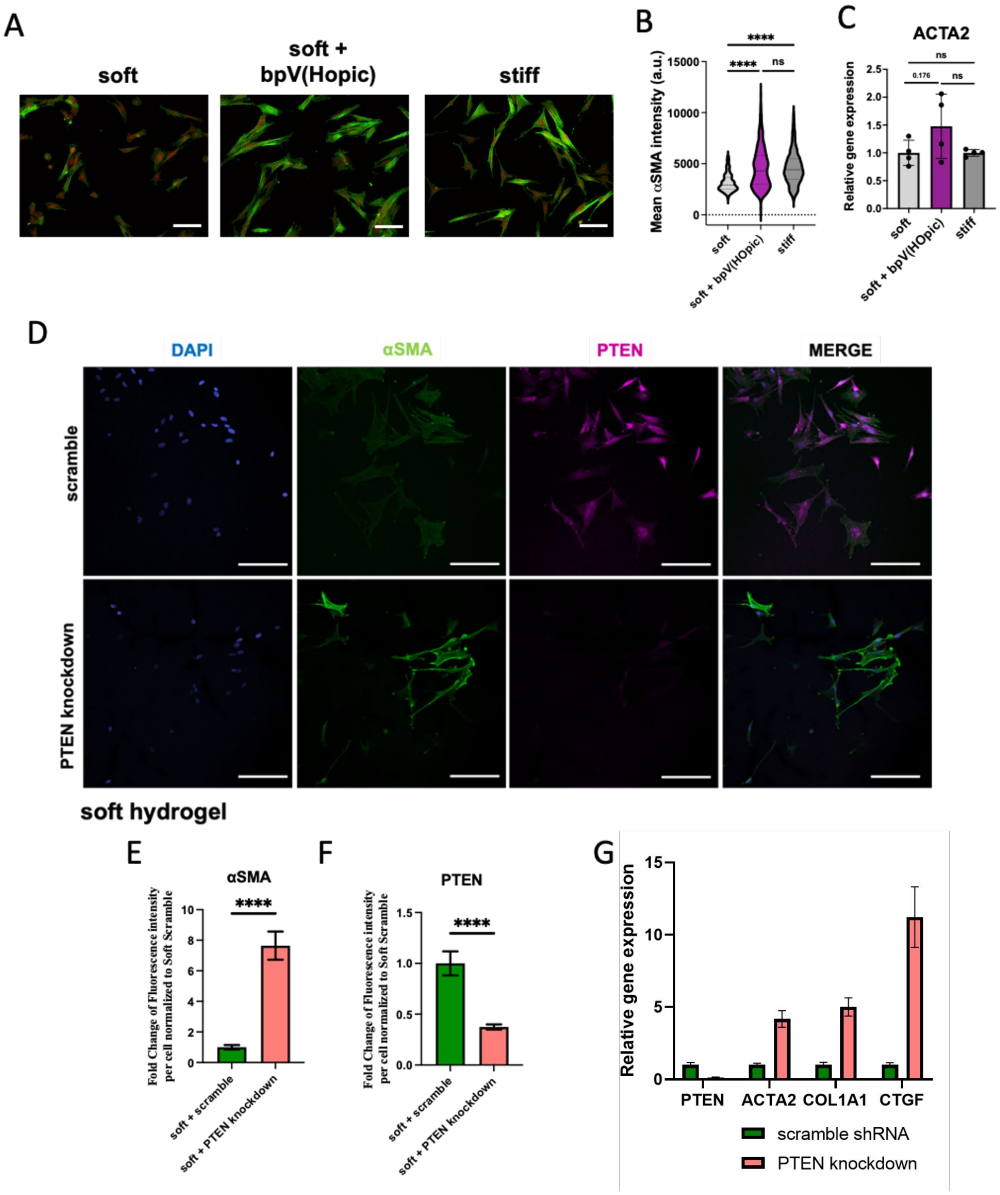

<u>Figure 4:</u> PTEN inhibitors increase myofibroblast activation in VICs. A. Representative images of VICs cultured on soft and stiff hydrogels for 3 days in the presence of DMSO vehicle or 100nM of PTEN inhibitor bpV(Hopic), αSMA (green) and cytoplasm(red). Scale bar = 100 µm. **B.** Quantification of αSMA intensity for A. (n>600 cells from 4 hydrogels, one-way ANOVA test, ****p<0.001). **C.** Relative mRNA expression levels of ACTA2 in VICs cultured on soft hydrogels with treatment of DMSO vehicle or 100nM of PTEN inhibitor bpV(Hopic), and stiff hydrogels, n=4 wells, means ± SD shown. **D.** Representative images of scrambled and PTEN knockdown VICs cultured on stiff hydrogels for 3 days, αSMA (green) and cytoplasm(red). Scale bar = 100 µm. **E.** Quantification of αSMA fluorescence intensity (n>30 cells, t-test ,****p<0.001) **F.** Quantification of PTEN fluorescence intensity (n>30 cells, t-test, ****p<0.001). **G.** Relative mRNA expression levels of various fibrotic genes in VICs treated with the scrambled or PTEN on TCPS, n=1 vector.

412
413 *High nuclear/cytoplasmic ratio of PTEN correlates with low αSMA levels in VIC on stiff hydrogels*
414
415 In addition to the canonical role of PTEN in dephosphorylating PIP3 at the cell membrane,
416 additional roles of PTEN and its nuclear localization have been recently identified, namely that
417 PTEN is able to act as a transcription factor and alter global chromatin architecture and gene
418 expression levels.[39] Further, we have previously shown that matrix stiffness can influence the
419 persistence of VIC myofibroblast activation through epigenetic remodeling, so we next sought to
420 test whether nuclear PTEN is involved in this process. Specifically, we used quantitative image
421 analysis to investigate the subcellular localization of PTEN in VICs cultured on both soft and stiff
422 hydrogels.
423 Initially, we quantified αSMA levels of VIC cultures on soft and stiff hydrogels and separated the
424 population into two classes: fibroblasts and myofibroblasts based on the intensity of αSMA signal.
425 We observed that the quiescent VIC fibroblasts had a significantly higher nuclear to cytoplasmic
426 PTEN ratio compared to myofibroblasts cultured on stiff hydrogels, where PTEN remained largely
427 cytoplasmic **(Figure 5 A,B)**. We observed no statistically significant differences in the
428 nuclear/cytoplasmic PTEN ratio between fibroblasts and myofibroblasts in VICs cultured on soft
429 hydrogels, where VICs are quiescent. **(Figure 5 C-D).** Together, these results suggest that PTEN
430 may serve an additional role in the nucleus, protecting against stiffness-induced matrix activation
431 of myofibroblasts.
432

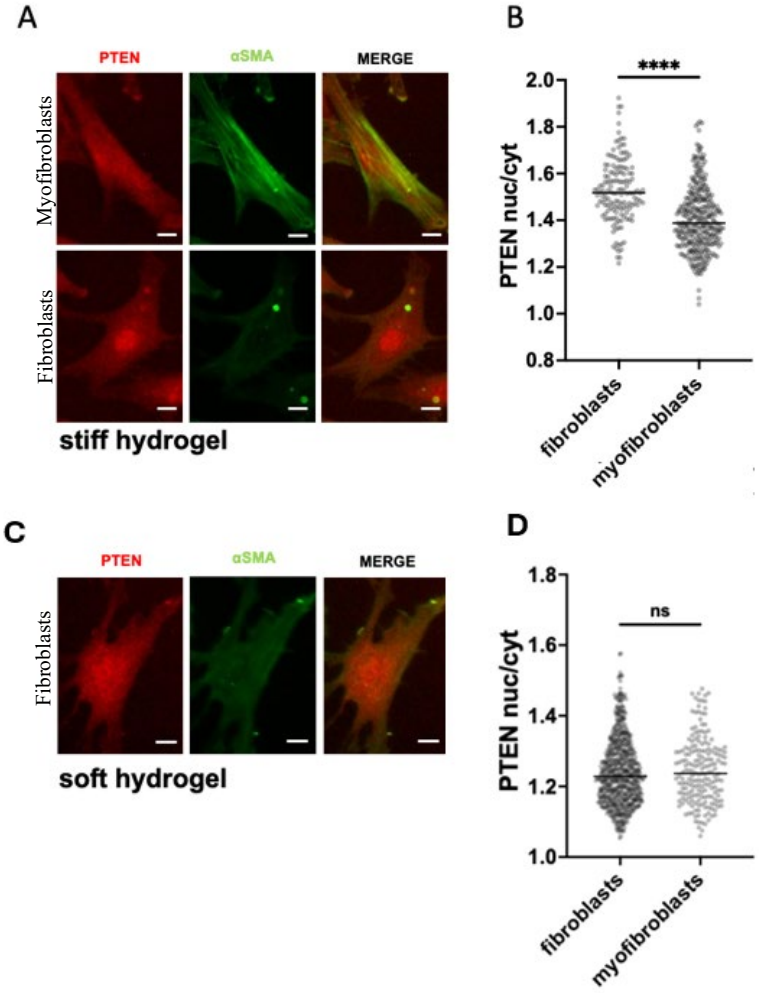

Figure 5: High nuclear/cytoplasmic ratio of PTEN correlates with low αSMA levels on stiff hydrogels. A. Single cell images of VICs cultured on stiff hydrogels for 3 days αSMA (green) and PTEN (red). Scale bar = 10 µm. B. Quantification of PTEN nuclear to cytoplasmic ratio in fibroblast and myofibroblast populations on stiff hydrogels (n>250 cells from 4 hydrogels, one-way ANOVA test, ****p<0.001). C. Single cell images of VICs cultured on soft hydrogels for 3 days αSMA (green) and PTEN (red). Scale bar = 10 µm. D. Quantification of PTEN nuclear to cytoplasmic ratio in fibroblast and myofibroblast populations on soft hydrogels (n>250 cells from 4 hydrogels, one-way ANOVA test, ****p<0.001). E. Quantification of nuclear area of cells with high and low nuclear to cytoplasmic PTEN ratio on soft hydrogels (n>250 cells from 4 hydrogels).

To verify the role of PTEN localization in myofibroblast activation, we ectopically expressed PTEN in VICs with two distinct nucleotide sequences that signal either nuclear (nuclear localization signal-NLS) or cytoplasmic (nuclear exclusion signal-NES) localization. Both

448 plasmid constructs contain a hemagglutinin (HA) tag to verify transfection efficiency. VICs were
449 plated on stiff 2D hydrogels and transfected with either NES PTEN or NLS PTEN plasmids with
450 ~4-7% efficiency **(Figure 6 D)**. After 3 days, we observed increased PTEN nuclear/cytoplasmic
451 ratio in the NLS PTEN condition compared to NES PTEN and untransfected control, indicating
452 that the transfected plasmid constructs localized PTEN as expected **(Figure 6 A, B)**. More
453 importantly, αSMA was significantly downregulated among the cells transfected with NLS PTEN,
454 while αSMA levels were slightly upregulated in the NES PTEN compared to untransfected control
455 **(Figure 6 A, C)**, indicating that nuclear PTEN plays a protective role against myofibroblast
456 activation on stiff hydrogels.

457 As nuclear PTEN has been shown to play a role in nuclear dynamics and epigenetic
458 modifications, we wanted to test if there was a correlation between high nuclear PTEN and nuclear
459 area in VICs.[39] For VICs cultured on stiff hydrogels, we separated the cell population into two
460 cohorts based on their nuclear to cytoplasmic PTEN ratio. VICs with a high nuclear/cytoplasmic
461 PTEN ratio (nuclear/ cytoplasmic PTEN ≥ than 1.5) had significantly smaller nuclei compared to
462 VICs with low nuclear/cytoplasmic PTEN ratio (nuclear/ cytoplasmic PTEN < than 1.5) **(Figure**
463 **6 E)**. This observation lead us to a more in depth investigation of the role of PTEN in chromatin
464 dynamics.
465

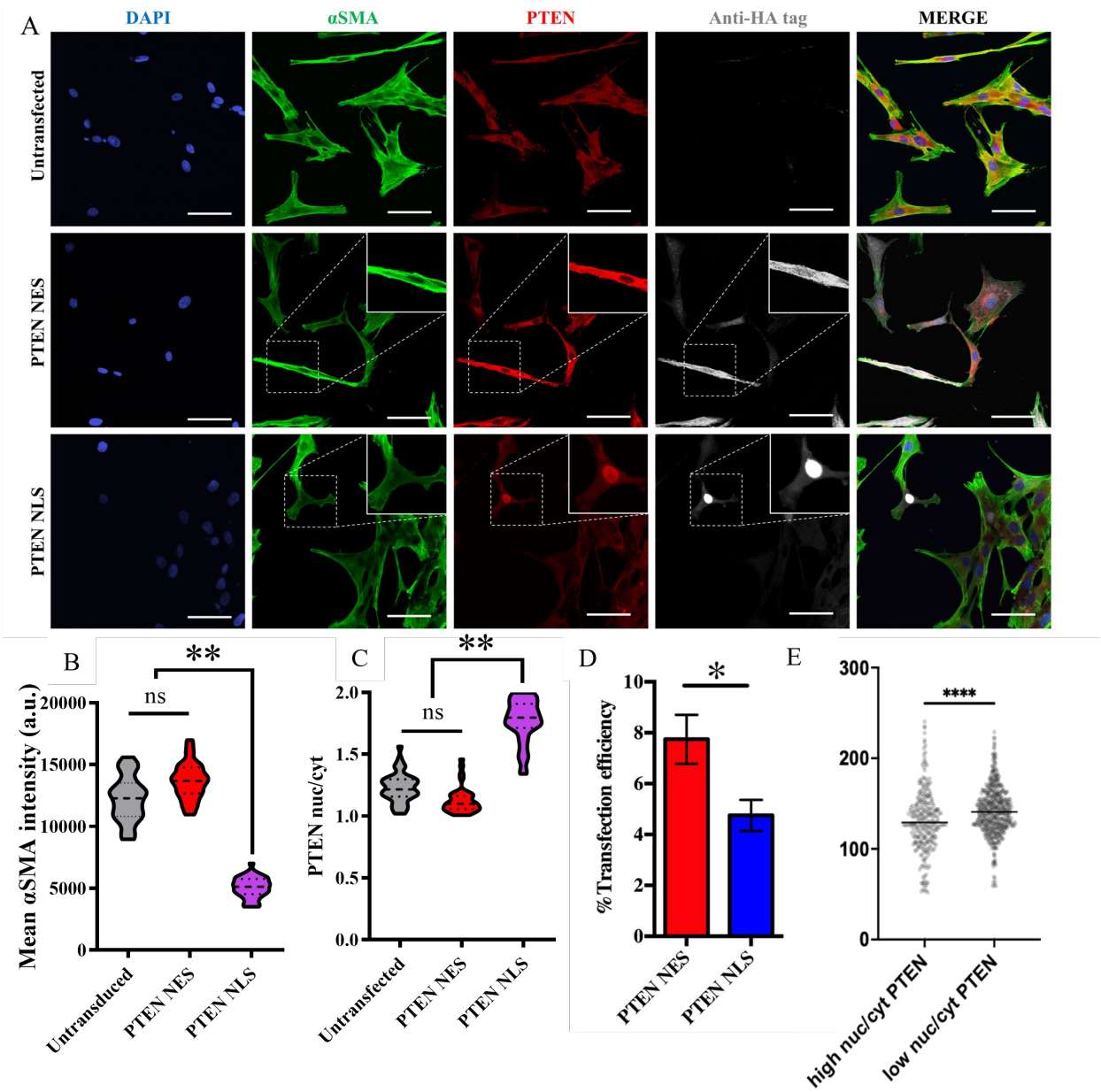

Figure 6: Ectopic expression of NLS PTEN downregulates αSMA on stiff hydrogels. A. Single cell images of VICs cultured on stiff hydrogels for 3 days αSMA (green), PTEN (red) and anti-HA tag (white). Scale bar = 10 µm. **B.** Quantification of αSMA among untransfected VICs and VICs with ectopic expression of NES and NLS PTEN on stiff hydrogels. (n=40 cells from 6 hydrogels, one-way ANOVA test, ****p<0.001) **C.** Quantification of the ratio of nuclear to cytoplasmic PTEN among untransfected, NES and NLS VICs (n=40 cells from 6 hydrogels, one-way ANOVA test, ****p<0.001). **D.** Quantification of the % transfection efficiency between NES and NLS PTEN. (n=40 cells from 6 hydrogels, one-way ANOVA test, ****p<0.001) **E.** Quantification of nuclear area of cells with high and low nuclear to cytoplasmic PTEN ratio on stiff hydrogels (n>250 cells from 4 hydrogels).

Since the nuclear/cytoplasmic ratio of PTEN affected nuclear size in addition to αSMA levels, we subsequently studied the effect of the localization of PTEN on VIC epigenetic modifications. PTEN has been implicated in the regulation of histone activity in the context of fibrosis and heart failure, thus, we were interested in the correlation between the protective role of PTEN against αSMA upregulation and the levels of the tri-methylation of histone 3 on lysine-9 (H3K9me3) on VICs cultured for 3 days on soft and stiff hydrogels transfected with NES PTEN

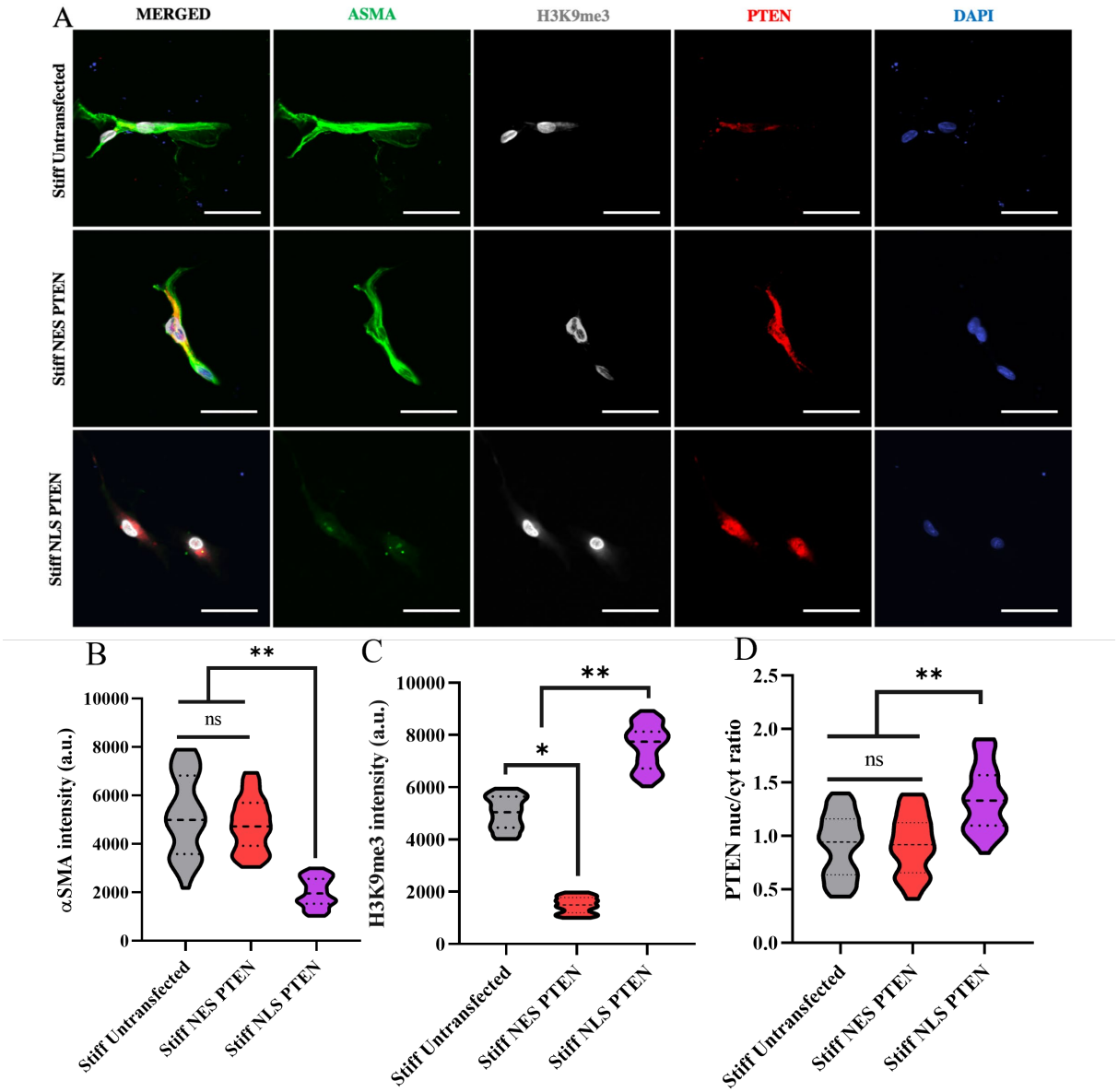

<u>Figure 7:</u> Nuclear localization of PTEN upregulates H3K9me3 on stiff hydrogels and protects against myofibroblast activation. A. Single cell immunocytochemical images of untransfected VICs and VICs with ectopic expression of NES and NLS PTEN cultured on stiff hydrogels for 3 days stained for αSMA (green), PTEN (red) and H3K9me3 (white). Scale bar = 10 µm. **B.** Quantification of αSMA intensity among untransfected VICs and VICs with ectopic expression of NES and NLS PTEN on stiff hydrogels. (n=50 cells from 4 hydrogels, one-way ANOVA test, ****$p<0.001$) **C.** Quantification of H3K9me3 nuclear intensity. (n=50 cells from 4 hydrogels, one-way ANOVA test, ****$p<0.001$) **D.** Quantification of the ratio of nuclear to cytoplasmic PTEN among untransfected, NES and NLS VICs (n=50 cells from 4 hydrogels, one-way ANOVA test, ****$p<0.001$).[40–42]

or NLS PTEN. Consistent with our previous results, the high nuclear/cytoplasmic ratio of PTEN, induced by NLS PTEN transfection, downregulated αSMA on stiff hydrogels but also upregulated H3K9me3, increasing its nuclear levels. In the NES PTEN as well as the untransfected control conditions, H3K9me3 levels remained significantly lower **(Figure 7A-D)**. Interestingly, on soft hydrogels, where VICs display low αSMA levels, the increase in nuclear/cytoplasmic PTEN ratio, similarly, resulted in increased H3K9me3 levels **(Supplementary Figure 9A-D)**. This, indicated that the PTEN-H3K9me3 upregulation modulates αSMA levels, but their interactions are independent of VIC myofibroblast activation.

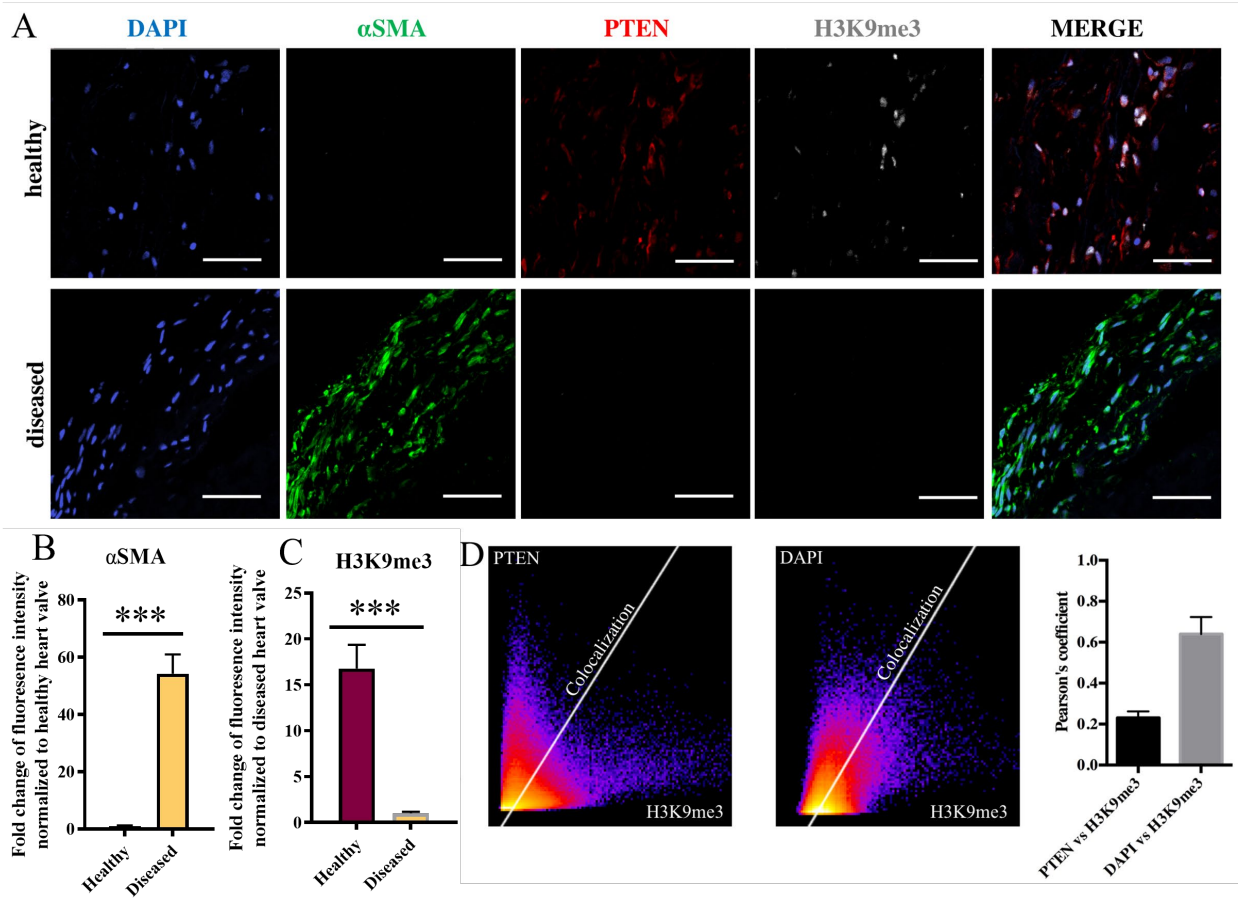

<u>Figure 8:</u> PTEN levels correlate with H3K8me3 levels in healthy human heart valve tissue while inversely correlating with αSMA on diseased tissue. A. Representative histological images of AVS and healthy human heart valve tissue (male) stained for DAPI (blue), αSMA (green), PTEN (red) and H3K9me3 (white) levels in valvular interstitial cells. Scale bar = 40 µm **B.** Quantification of average αSMA intensity (normalized to DAPI per mm^2) for healthy and diseased tissue. (normalized to DAPI per mm^2, n=5 fields of view per tissue, 2 biological replicates, t-test, ***$p<0.001$). **C.** Quantification of average H3K9me3 intensity (normalized to DAPI per mm^2) for healthy and diseased tissue. (normalized to DAPI per mm^2, n=5 fields of view per tissue, 2 biological replicates, t-test, ***$p<0.001$). **D.** Colocalization analysis of H3K9me3 and DAPI and αSMA. Plot of the classical Pearson's coefficient. (n=5 fields of view per tissue, 2 biological replicates)

Finally, we were interested in the translation of our *in vitro* results of the PTEN-H3K9me3 interactions on human healthy and fibrotic heart valve tissue. Interestingly, histological analysis positively correlated the levels of PTEN with the levels of H3K9me3 in healthy tissue and

523 inversely correlated with αSMA levels in fibrotic tissue **(Figure 8 A-C)**. Colocalization analysis
524 of H3K9me3 with DAPI, confirmed its nuclear localization albeit H3K9me3 only partially
525 localizing with PTEN in human tissues **(Figure 8 D)**, suggesting an important but complex role of
526 PTEN in the regulation of αSMA in human heart valve tissue.

527

528 **Discussion**

529

530 Results presented herein suggest that PTEN regulates myofibroblast activation in VICs,
531 which is consistent with the emerging notion that PTEN plays a central protective role against
532 fibrosis development in numerous tissues and organ systems.[25–27,29,36] as well as myogenic
533 differentiation of smooth vascular smooth muscle cells[62]. In line with this, we observed decreased
534 levels of PTEN in diseased human valve leaflet tissues compared to healthy ones. The results
535 linking PTEN with aortic valve stenosis complement what has been shown in tissue samples from
536 patients with pulmonary fibrosis, where an inverse correlation of the expression of PTEN and
537 αSMA was observed.[43] Further, loss of PTEN protein and downregulation in its phosphatase
538 activity have both been linked to development of pulmonary fibrosis.[44–48] To further investigate
539 the role of PTEN, we exploited biomaterial matrices to study the cross-talk between
540 mechanosensing and matrix signaling, in the absence of other confounding factors, that can
541 influence the VIC fibroblast-to-myofibroblast transition. We focused on elucidating how
542 regulation of PTEN activity alters VIC activation/quiescence in both soft (healthy) and stiff
543 (fibrotic-like) hydrogel microenvironments. Our findings suggest that PTEN has multiple modes
544 of action depending on PTEN localization and matrix stiffness **(Figure 9)**. We observe total PTEN
545 expression levels decrease with matrix stiffness, inverse to the effects of stiffness on VIC
546 myofibroblast activation. However, the spatial distribution of PTEN matters, as high nuclear to
547 cytoplasmic ratio of PTEN on stiff hydrogels correlates with the quiescent fibroblast phenotype,

548 as observed in **Figure 5** and may protect against myofibroblast activation when VICs are grown

549 in stiff, fibrotic-like microenvironments.

550

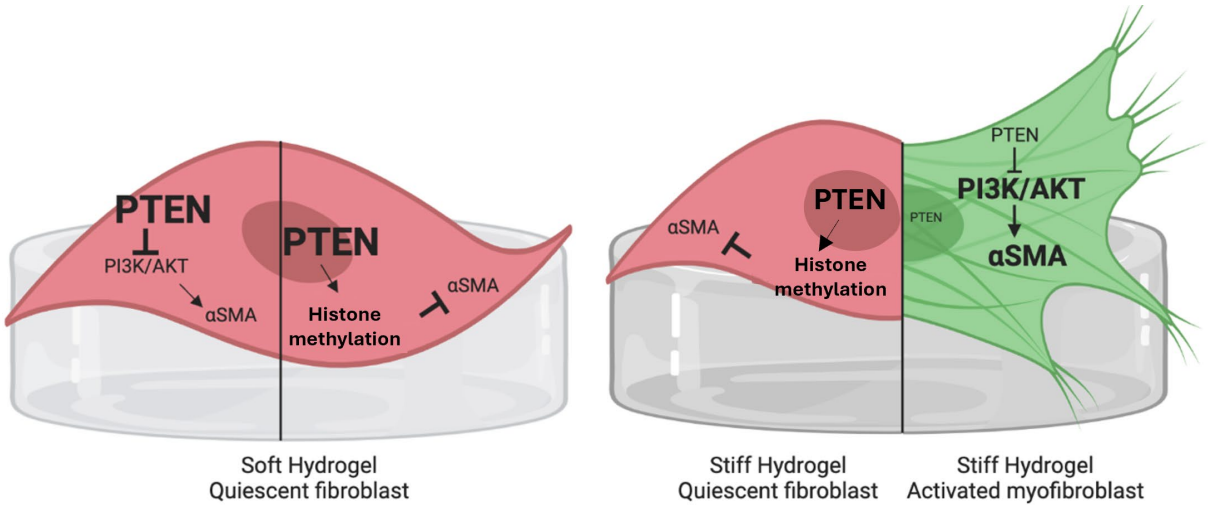

551

552

553 **<u>Figure 9:</u> Schematic of PTEN activity in VICs on soft and stiff hydrogels. A.** VICs cultured
554 on soft hydrogels are quiescent due to the high PTEN activity in both the cellular cytosol and
555 nucleus. Cytosolic PTEN acts as an antagonist of PI3K/AKT, while nuclear PTEN is involved in
556 the regulation of histone expression. **B.** VICs differentiate towards myofibroblasts on stiff
557 hydrogels due to the downregulation of PTEN, resulting in increased levels of phosphor-
558 PI3K/AKT and elevated αSMA expression levels. However, when PTEN is ectopically expressed
559 in the nucleus, αSMA levels are downregulated through increased expression of H3K9me3,
560 maintaining VIC quiescence.
561

562 Further, we show that PTEN directly influences myofibroblast activation in VICs. PTEN

563 is a known inhibitor of the PI3K/AKT pathway, and results from our lab reported by Wang *et al.*

564 have shown that the phosphorylation of PI3K/AKT pathway is central to matrix stiffness induced

565 myofibroblast activation in VICs.[24] We validate the involvement of AKT in myofibroblast

566 activation by pharmacological inhibition of phospho-AKT through MK-2206, which resulted in

567 decreased αSMA levels. This led us to examine the relative role of PTEN, an AKT antagonist,

568 abrogating the effects of mechanosensing. Namely, PTEN activators decrease, while PTEN

569 inhibitors increase myofibroblast activation, respectively. Furthermore, in addition to being

570 regulated by matrix stiffness, PTEN levels are also epigenetically regulated. We have
571 demonstrated increased mRNA expression of PTEN by 5-azacytidine and itraconazole treatment
572 (**Figure 3**, **Supplementary Figure 5**). Epigenetic silencing of PTEN has been proposed by
573 methylation of the CpG islands within the promoter, which is involved in several cancers.[49–53] As
574 such, methyltransferase inhibitors 5-azacytidine and decitabine have been previously identified as
575 PTEN activators by blocking methylation of the promoter and increasing gene expression.[28,54]
576 Interestingly, global methylation levels are reported to increase in AVS, which suggests that DNA
577 methylation inhibitors might also be used to reverse this process.[55]

578 While relative cell PTEN levels are strong indicators of myofibroblast activation in this
579 study and others, subcellular localization of PTEN has also been shown to play important roles in
580 influencing cell phenotype.[43,56–58] We observe that high nuclear localization of PTEN correlates
581 with the quiescent fibroblast phenotype and smaller nuclei for VICs on stiff gels, but no
582 correlations were observed with VICs on soft hydrogels. This suggests high nuclear localization
583 of PTEN may protect against myofibroblast activation. Although loss of PTEN has been
584 associated with fibrosis, subcellular localization of PTEN to the nucleus has not been previously
585 studied in relation to fibrotic disease. To investigate the role of PTEN nuclear localization in
586 myofibroblast activation, we ectopically expressed NES and NLS PTEN in VICs grown on stiff
587 substrates, where nuclear PTEN significantly downregulated αSMA expression. A high level of
588 nuclear PTEN, regulating epigenetic modifications, might suggest resistance to the transient
589 myofibroblast state and continued protection against activation.

590 Complementing this observation, recent work from our lab linked histone regulation and
591 chromatin condensation with myofibroblast activation.[19,59] Specifically, Walker *et al.* used ATAC-
592 seq to show that transient myofibroblasts have a more open chromatin structure, which

593 subsequently condenses again to the stabilized phenotypic condition.[59,19] PTEN has been shown
594 to interact with chromatin by directly binding to histone H1 and controlling epigenetic
595 modifications[60] , while nuclear PTEN levels correlate with H3K9me3 intensity, a marker for
596 chromatin condensation, and depletion of H3K9me3 is observed in PTEN knockout cells.[56]
597 Further, our results are consistent with PTEN levels *in vivo* that correlate with H3K9me3 levels
598 and potentially a protective effect against αSMA upregulation and fibrosis. Mechanistically, PTEN
599 may reinforce the H3K9me3 suppression of the PPARγ gene, decreasing the expression of fibrotic
600 markers such as αSMA and COL1.[61] Taken together, we propose that nuclear PTEN promotes the
601 VIC quiescent fibroblast phenotype by indirectly controlling αSMA expression at an epigenetic
602 level. However, the mechanism that leads to the heterogeneity of nuclear PTEN observed in the
603 VIC population remains a topic for future investigation.

604 In conclusion, we have shown that PTEN and its subcellular localization play an important
605 role in regulating myofibroblast activation in VICs. Increased global levels of PTEN expression,
606 either by low matrix stiffness or by pharmacological treatment, protect against myofibroblast
607 activation. High levels of nuclear PTEN correlate with a H3K9me2 expression levels and the
608 quiescent fibroblast phenotype, even on stiff hydrogel matrices. Importantly, this correlation is
609 recapitulated in human healthy and fibrotic heart valve tissues, where we have observed mutually
610 exclusive expression of αSMA and PTEN. Thus, we demonstrated that PTEN may be a valuable
611 pharmacological target for non-invasive therapeutics for valve fibrosis and lead to further
612 understanding of the dynamics of AVS progression.

613

614 **Acknowledgments:** We thank Dr. Robert Weiss for valuable discussions and feedback. We
615 acknowledge National Institutes of Health R01 HL142935 and R01 HL132353 awarded to KSA.

Author contributions: D.B., G.T., and K.S.A. designed and performed all the experiments. B.K. and A.K. performed image analysis, mathematical analysis, and data 32 analysis. D.B., B.E.K., G.T., K.B., M.W.E. and K.S.A. contributed to writing and editing the paper.

Competing interests: The authors report no competing interests.

Supplementary Material

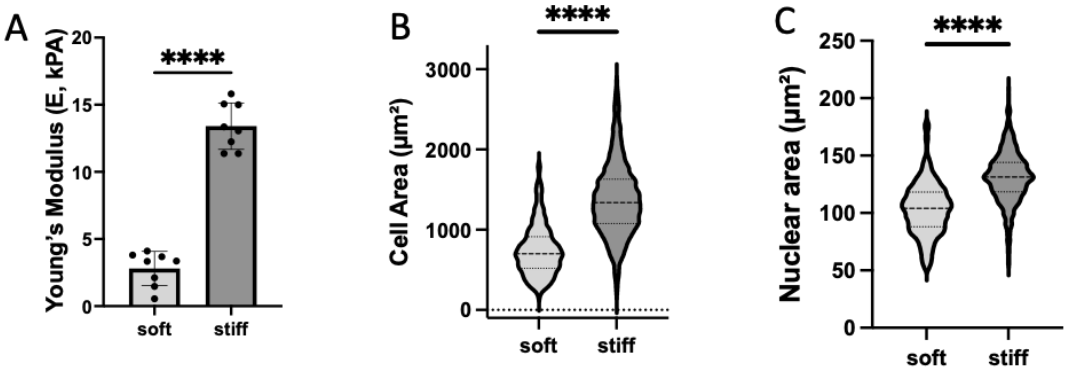

<u>Supplementary Figure 1:</u> VICs display increased cellular and nuclear area on stiff hydrogels. **A.** Young's modulus for synthesized soft and stiff swollen hydrogels by shear rheology. (n = 8, unpaired t test, ****p < .001). **B.** Quantification of cell size of VICs cultured on soft or stiff hydrogels for 3 days (n>740 cells from 4 hydrogels, unpaired t test, ****p<0.001). **C.** Quantification of nuclear area of VICs cultured on soft or stiff hydrogels for 3 days (n>740 cells from 4 hydrogels, unpaired t test, ****p<0.001).

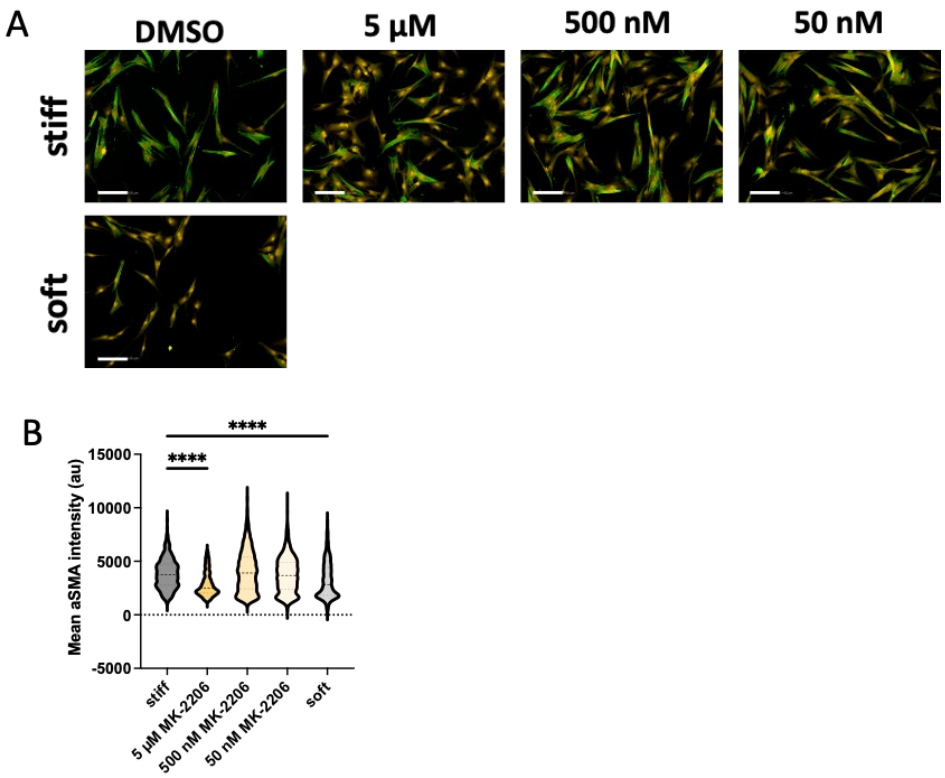

<u>Supplementary Figure 2:</u> VICs display decreased myofibroblast activation with AKT inhibition A. Representative images of VICs cultured on soft and stiff hydrogels for 3 days, αSMA (green) and cytoplasm (yellow). Scale bar = 100 µm **B.** Quantification of αSMA (green) intensity for A. (n>1000 cells from 4 hydrogels, one-way ANOVA test, ****p<0.001).

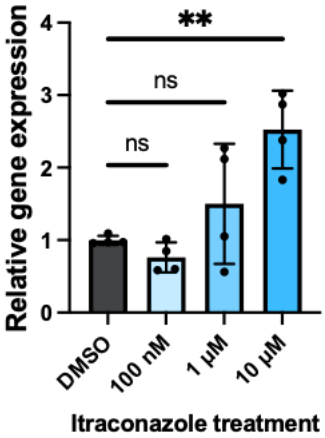

<u>Supplementary Figure 3:</u> Itraconazole treatment increases PTEN gene expression. Relative mRNA expression levels of PTEN in VICs cultured on TCPS with treatment of vehicle or increasing concentration of PTEN activator itraconazole, n=4 wells, means ± SD shown, one-way ANOVA test, **p < .01.

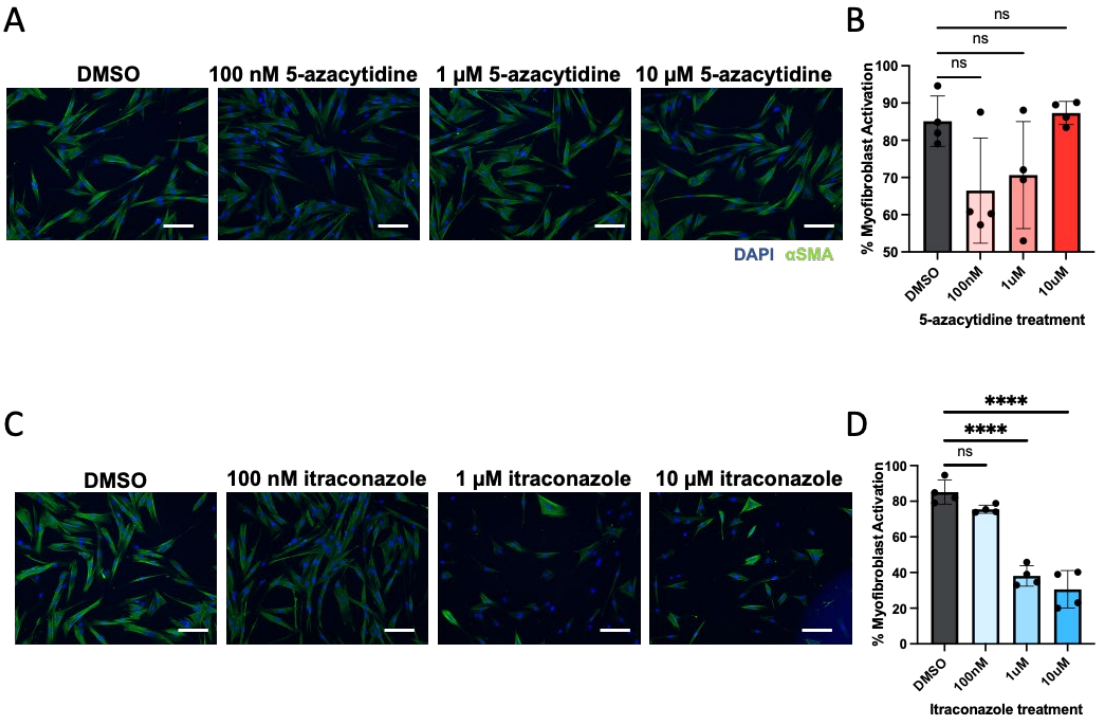

<u>Supplementary Figure 4:</u> PTEN activators decrease myofibroblast activation in VICs A. Representative images of VICs cultured on TCPS for 3 days with indicated concentrations of PTEN activators 5-azacytidine, αSMA (green) and nuclei(DAPI). Scale bar = 100 µm. **B.** Quantification of myofibroblast activation for A, n=4 wells, one-way ANOVA test. **C.** Representative images of VICs cultured on TCPS for 3 days with indicated concentrations of PTEN activators itraconazole, αSMA (green) and nuclei(DAPI). Scale bar = 100 µm. **D.** Quantification of myofibroblast activation for C, n=4 wells, one-way ANOVA test, ****p<0.001.

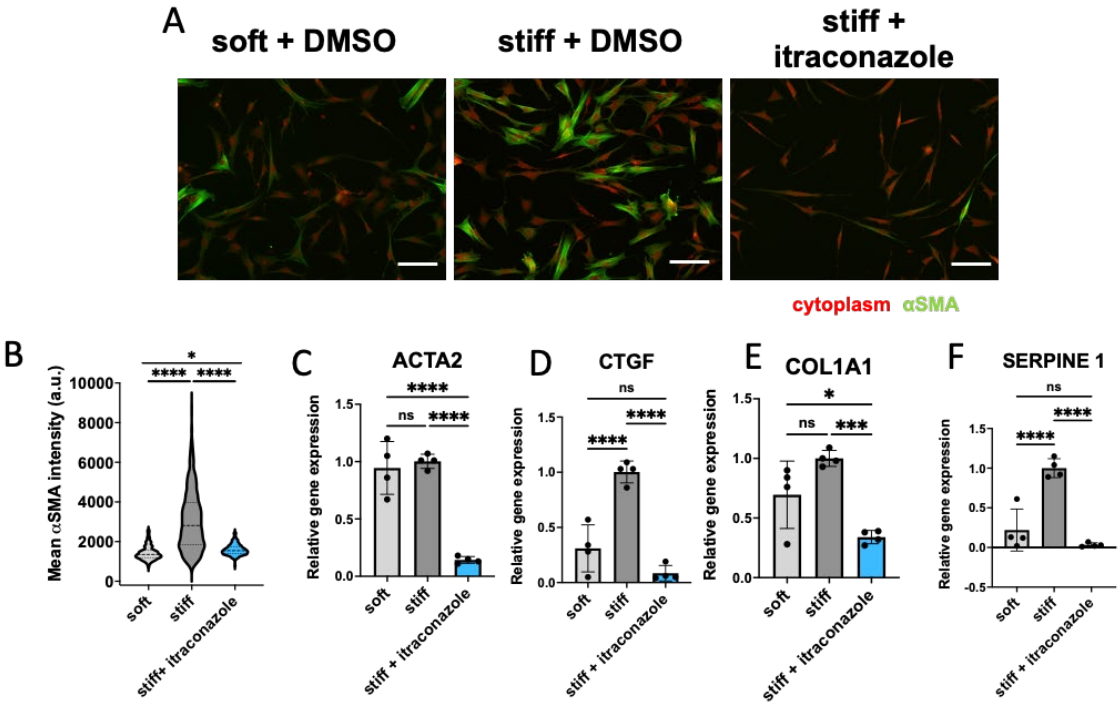

<u>Supplementary Figure 5:</u> PTEN activators decrease myofibroblast activation in VICs A. Representative images of VICs cultured on soft and stiff hydrogels for 3 days in the presence of DMSO vehicle or10 µM itraconazole (PTEN activator), αSMA (green) and cytoplasm(red). Scale bar = 100 µm. **B.** Quantification of αSMA intensity for A. (n>600 cells from 4 hydrogels, one-way ANOVA test, *p < .05, ****p<0.001). **C-F.** Relative mRNA expression levels of various fibrotic genes in VICs cultured on soft or stiff hydrogels treated with DMSO vehicle or PTEN activator itraconazole (10µM), n=4 hydrogels, one-way ANOVA test, *p < .05 ,**p < .01, ***p < .001,****p<0.001.

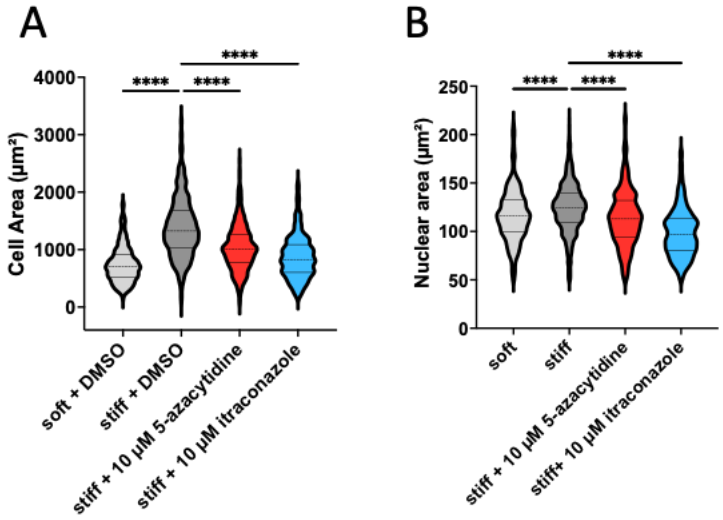

<u>Supplementary Figure 6:</u> PTEN activators decrease cellular and nuclear area of VICs cultured on stiff hydrogels. A. Quantification of cell size of VICs cultured on soft or stiff hydrogels for 3 days (n>600 cells from 4 hydrogels, unpaired t test, ****p<0.001). **B.** Quantification of cell size of VICs cultured on soft or stiff hydrogels for 3 days (n>600 cells from 4 hydrogels, unpaired t test, ****p<0.001).

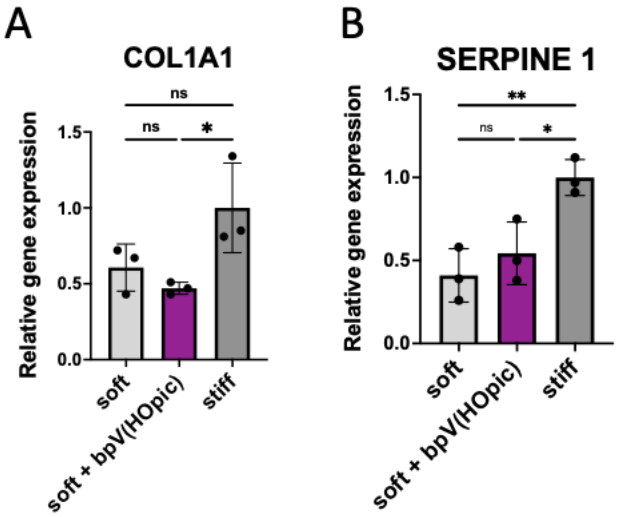

<u>Supplementary Figure 7:</u> PTEN phosphatase inhibition does not increase mRNA levels of fibrotic genes A,B. Relative mRNA expression levels of various fibrotic genes in VICs cultured on soft or stiff hydrogels treated with DMSO vehicle or PTEN inhibitor bpV(Hopic) (100 nM), n=3 hydrogels, one-way ANOVA test, *p < .05 ,**p < .01.

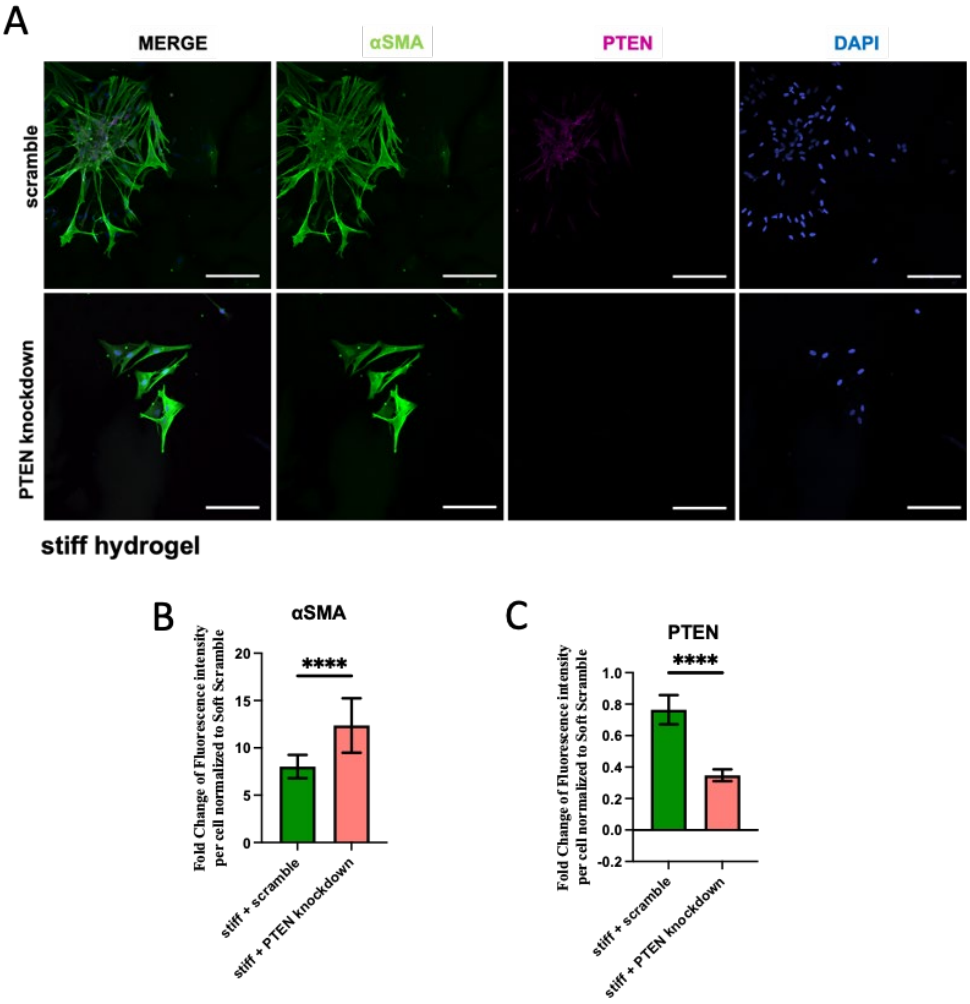

<u>Supplementary Figure 8:</u> PTEN knockdown increases αSMA levels in VICs cultured on stiff hydrogels A. Representative images of scrambled and PTEN knockdown VICs cultured on stiff hydrogels for 3 days, αSMA (green) and cytoplasm(red). Scale bar = 100 µm. **B.** Quantification of αSMA fluorescence intensity (n>30 cells, t-test ,****p<0.001) **C.** Quantification of PTEN fluorescence intensity (n>30 cells, t-test, ****p<0.001).

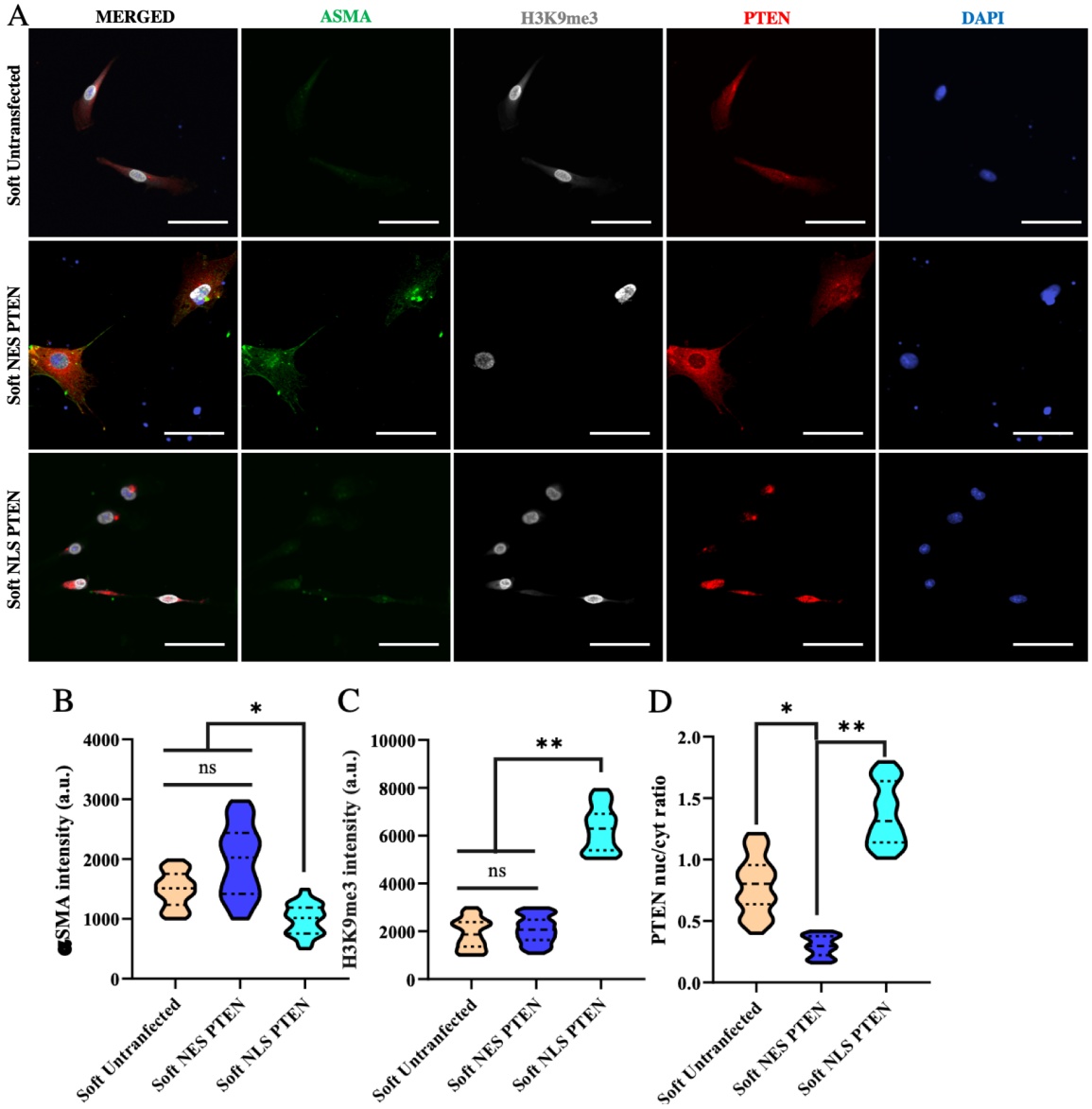

<u>Supplementary Figure 9:</u> Nuclear localization of PTEN upregulates H3K9me3 on soft hydrogels. A. Single cell immunocytochemical images of VICs cultured on soft hydrogels for 3 days αSMA (green), PTEN (red) and H3K9me3 (white). Scale bar = 10 µm. **B.** Quantification of αSMA intensity among untransfected VICs and VICs with ectopic expression of NES and NLS PTEN on soft hydrogels. (n=50 cells from 4 hydrogels, one-way ANOVA test, ****p<0.001) **C.** Quantification of H3K9me3 nuclear intensity. (n=50 cells from 4 hydrogels, one-way ANOVA test, ****p<0.001) **D.** Quantification of the ratio of nuclear to cytoplasmic PTEN among untransfected, NES and NLS VICs (n=50 cells from 4 hydrogels, one-way ANOVA test, ****p<0.001).

717

718

719 **<u>Table S1:</u> Custom Primers used for RT-qPCR**

GENE:	FW sequence 5′ to 3′	RV sequence 5′ to 3′
PTEN	GGCGGAACTTGCAATCCTCA	AACTTGTCTTCCCGTCGTGT
L30	GCTGGGGTACAAGCAGACTC	AGATTTCCTCAAGGCTGGGC
COL1A1	GGGCAAGACAGTGATTGAATACA	GGATGGAGGGAGTTTACAGGAA
CTGF	CTGGTCCAGACCACAGAGTGG	GCAGAAAGCGTTGTCATTGG
ACTA2	GCAAACAGGAATACGATGAAGCC	AACACATAGGTAACGAGTCAGAGC
SERPINE 1	ACGGCCATTATCGTCTCAGC	AAAAGGACCGTTCCTGTGGG

720

721

722 **<u>Table S2:</u> Patient Information of the tissue used**

Condition	Age	Sex	Race (Ethnicity)	Diagnosis	LVEF (%)
Healthy	45	M	american indian	non-ischemic	35
Stenotic	67	M	W	ischemic	29.5

723

724

725 **References**
726

727 1. Otto CM, Prendergast B. Aortic-Valve Stenosis — From Patients at Risk to Severe Valve
728 Obstruction. *N Engl J Med*. 2014;371:744–756.
729 2. Yutzey KE, Demer LL, Body SC, Huggins GS, Towler DA, Giachelli CM, Hofmann-
730 Bowman MA, Mortlock DP, Rogers MB, Sadeghi MM, Aikawa E. Calcific aortic valve
731 disease: A consensus summary from the alliance of investigators on calcific aortic valve
732 disease. *Arterioscler Thromb Vasc Biol*. 2014;34:2387–2393.
733 3. Schlotter F, Halu A, Goto S, Blaser MC, Body SC, Lee LH, Higashi H, DeLaughter DM,
734 Hutcheson JD, Vyas P, Pham T, Rogers MA, Sharma A, Seidman CE, Loscalzo J,
735 Seidman JG, Aikawa M, Singh SA, Aikawa E. Spatiotemporal Multi-Omics Mapping
736 Generates a Molecular Atlas of the Aortic Valve and Reveals Networks Driving Disease.
737 *Circulation* [Internet]. 2018;138:377–393. Available from:
738 https://www.ahajournals.org/doi/10.1161/CIRCULATIONAHA.117.032291
739 4. Goody PR, Hosen MR, Christmann D, Niepmann ST, Zietzer A, Adam M, Bönner F,
740 Zimmer S, Nickenig G, Jansen F. Aortic valve stenosis: From basic mechanisms to novel
741 therapeutic targets. *Arterioscler Thromb Vasc Biol*. 2020;885–900.
742 5. Liang F, Wang X, Wang Q, Yan P, Yao L. Predilatation and paravalvular leakage risk in
743 TAVR. *Lancet* [Internet]. 2020;396:600. Available from: http://dx.doi.org/10.1016/S0140-
744 6736(20)30624-3
745 6. Liu AC, Joag VR, Gotlieb AI. The emerging role of valve interstitial cell phenotypes in
746 regulating heart valve pathobiology. *Am J Pathol* [Internet]. 2007;171:1407–1418.
747 Available from: http://dx.doi.org/10.2353/ajpath.2007.070251
748 7. Kendall RT, Feghali-Bostwick CA. Fibroblasts in fibrosis: Novel roles and mediators.
749 *Front Pharmacol*. 2014;5 MAY:1–13.
750 8. Humphrey JD, Dufresne ER, Schwartz MA. Mechanotransduction and extracellular
751 matrix homeostasis. *Nat Rev Mol Cell Biol* [Internet]. 2014;15:802–812. Available from:
752 http://dx.doi.org/10.1038/nrm3896
753 9. Hinz B. Myofibroblasts. *Exp Eye Res* [Internet]. 2016;142:56–70. Available from:
754 http://www.ncbi.nlm.nih.gov/pubmed/26192991
755 10. Duscher D, Maan ZN, Wong VW, Rennert RC, Januszyk M, Rodrigues M, Hu M,
756 Whitmore AJ, Whittam AJ, Longaker MT, Gurtner GC. Mechanotransduction and
757 fibrosis. *J Biomech* [Internet]. 2014;47:1997–2005. Available from:
758 http://www.nature.com/articles/ncb2756
759 11. Wang H, Leinwand LA, Anseth KS. Cardiac valve cells and their microenvironment-
760 insights from in vitro studies. Nat. Rev. Cardiol. 2014;11:715–727.
761 12. Ceccato TL, Starbuck RB, Hall JK, Walker CJ, Brown TE, Killgore JP, Anseth KS,
762 Leinwand LA. Defining the Cardiac Fibroblast Secretome in a Fibrotic
763 Microenvironment. *J Am Heart Assoc*. 2020;9:e017025.
764 13. Kuehlmann B, Bonham CA, Zucal I, Prantl L, Gurtner GC. Mechanotransduction in
765 Wound Healing and Fibrosis. *J Clin Med*. 2020;9:1423.
766 14. Ma H, Macdougall LJ, GonzalezRodriguez A, Schroeder ME, Batan D, Weiss RM,
767 Anseth KS. Calcium Signaling Regulates Valvular Interstitial Cell Alignment and
768 Myofibroblast Activation in Fast-Relaxing Boronate Hydrogels. *Macromol Biosci*.
769 2020;20:1–14.
770 15. Batan D, Peters DK, Schroeder ME, Aguado BA, Young MW, Weiss RM, Anseth KS.

Hydrogel cultures reveal Transient Receptor Potential Vanilloid 4 regulation of myofibroblast activation and proliferation in valvular interstitial cells. *FASEB J* [Internet]. 2022 [cited 2023 Jan 5];36:1–16. Available from: https://onlinelibrary.wiley.com/doi/full/10.1096/fj.202101863R

16. Caliari SR, Burdick JA. A practical guide to hydrogels for cell culture. *Nat Methods 2016 135* [Internet]. 2016 [cited 2023 Jan 10];13:405–414. Available from: https://www.nature.com/articles/nmeth.3839
17. Tibbitt MW, Anseth KS. Hydrogels as extracellular matrix mimics for 3D cell culture. *Biotechnol Bioeng* [Internet]. 2009 [cited 2023 Jan 10];103:655–663. Available from: https://onlinelibrary-wiley-com.colorado.idm.oclc.org/doi/full/10.1002/bit.22361
18. Mann BK, Gobin AS, Tsai AT, Schmedlen RH, West JL. Smooth muscle cell growth in photopolymerized hydrogels with cell adhesive and proteolytically degradable domains: Synthetic ECM analogs for tissue engineering. *Biomaterials*. 2001;22:3045–3051.
19. Walker CJ, Batan D, Bishop CT, Ramirez D, Aguado BA, Schroeder ME, Crocini C, Schwisow J, Moulton K, Macdougall L, Weiss RM, Allen MA, Dowell R, Leinwand LA, Anseth KS, Leslie Leinwand CA. Extracellular matrix stiffness controls cardiac valve myofibroblast activation through epigenetic remodeling. *Bioeng Transl Med*. 2022;7.
20. Grim JC, Aguado BA, Vogt BJ, Batan D, Andrichik CL, Schroeder ME, Gonzalez-Rodriguez A, Max Yavitt F, Weiss RM, Anseth KS. Secreted factors from proinflammatory macrophages promote an osteoblast-like phenotype in valvular interstitial cells. *Arterioscler Thromb Vasc Biol*. 2020;E296–E308.
21. Aguado BA, Walker CJ, Grim JC, Schroeder ME, Batan D, Vogt BJ, Rodriguez AG, Schwisow JA, Moulton KS, Weiss RM, Heistad DD, Leinwand LA, Anseth KS. Genes That Escape X Chromosome Inactivation Modulate Sex Differences in Valve Myofibroblasts. *Circulation*. 2022;145:513–530.
22. Kloxin AM, Benton JA, Anseth KS. In situ elasticity modulation with dynamic substrates to direct cell phenotype. *Biomaterials* [Internet]. 2010 [cited 2023 Jan 10];31:1. Available from: /pmc/articles/PMC2791128/
23. Wang J, Hu K, Cai X, Yang B, He Q, Wang J, Weng Q. Targeting PI3K/AKT signaling for treatment of idiopathic pulmonary fibrosis. *Acta Pharm Sin B* [Internet]. 2022 [cited 2023 Feb 2];12:18–32. Available from: www.elsevier.com/locate/apsbwww.sciencedirect.com
24. Wang H, Tibbitt MW, Langer SJ, Leinwand LA, Anseth KS. Hydrogels preserve native phenotypes of valvular fibroblasts through an elasticity-regulated PI3K/AKT pathway. *Proc Natl Acad Sci U S A* [Internet]. 2013;110:19336–19341. Available from: http://www.pnas.org/content/110/48/19336.short%7B%5C%25%7D5Cnhttp://www.ncbi.nlm.nih.gov/pubmed/24218588
25. Cai B, Yang L, Jung Y Do, Zhang Y, Liu X, Zhao P, Li J. PTEN: An Emerging Potential Target for Therapeutic Intervention in Respiratory Diseases. 2022 [cited 2022 Dec 8];Available from: https://doi.org/10.1155/2022/4512503
26. Lu S, Strand KA, Mutryn MF, Tucker RM, Jolly AJ, Furgeson SB, Moulton KS, Nemenoff RA, Weiser-Evans MCM. PTEN (phosphatase and tensin homolog) protects against ang II (angiotensin II)-induced pathological vascular fibrosis and remodeling - Brief report. *Arterioscler Thromb Vasc Biol*. 2020;40:394–403.
27. Parapuram SK, Thompson K, Tsang M, Hutchenreuther J, Bekking C, Liu S, Leask A. Loss of PTEN expression by mouse fibroblasts results in lung fibrosis through a CCN2-

817 dependent mechanism. *Matrix Biol*. 2015;43:35–41.
818 28. Strand KA, Lu S, Mutryn MF, Li L, Zhou Q, Enyart BT, Jolly AJ, Dubner AM, Moulton
819 KS, Nemenoff RA, Koch KA, Labarbera D V., Weiser-Evans MCM. High throughput
820 screen identifies the DNMT1 (DNA Methyltransferase-1) inhibitor, 5-azacytidine, as a
821 potent inducer of PTEN (Phosphatase and Tensin Homolog): Central Role for PTEN in 5-
822 azacytidine protection against pathological vascular remodeling. *Arterioscler Thromb*
823 *Vasc Biol*. 2020;40:1854–1869.
824 29. Parapuram SK, Shi-Wen X, Elliott C, Welch ID, Jones H, Baron M, Denton CP, Abraham
825 DJ, Leask A. Loss of PTEN Expression by Dermal Fibroblasts Causes Skin Fibrosis. *J*
826 *Invest Dermatol*. 2011;131:1996–2003.
827 30. Jones CE, Sharick JT, Colbert SE, Shukla VC, Zent JM, Ostrowski MC, Ghadiali SN,
828 Sizemore ST, Leight JL. Pten regulates collagen fibrillogenesis by fibroblasts through
829 SPARC. *PLoS One* [Internet]. 2021;16:1–21. Available from:
830 http://dx.doi.org/10.1371/journal.pone.0245653
831 31. Kloxin AM, Kasko AM, Salinas CN, Anseth KS. Photodegradable hydrogels for dynamic
832 tuning of physical and chemical properties. *Science (80-)*. 2009;324:59–63.
833 32. Yang C, Tibbitt MW, Basta L, Anseth KS. Mechanical memory and dosing influence stem
834 cell fate. *Nat Mater*. 2014;13:645–652.
835 33. Mehrotra P, Ikhapoh I, Lei P, Tseropoulos G, Zhang Y, Wang J, Liu S, Bronner ME,
836 Andreadis ST. Wnt/BMP Mediated Metabolic Reprogramming Preserves Multipotency of
837 Neural Crest-Like Stem Cells. *Stem Cells* [Internet]. 2023 [cited 2023 May 5];41:287–
838 305. Available from: https://academic.oup.com/stmcls/article/41/3/287/6976057
839 34. Malkomes P, Lunger I, Luetticke A, Oppermann E, Haetscher N, Serve H, Holzer K,
840 Bechstein WO, Rieger MA. Selective AKT Inhibition by MK-2206 Represses Colorectal
841 Cancer-Initiating Stem Cells. *Ann Surg Oncol* [Internet]. 2016 [cited 2023 May
842 14];23:2849–2857. Available from: https://pubmed.ncbi.nlm.nih.gov/27059026/
843 35. Liu R, Liu D, Trink E, Bojdani E, Ning G, Xing M. The Akt-specific inhibitor MK2206
844 selectively inhibits thyroid cancer cells harboring mutations that can activate the PI3K/Akt
845 pathway. *J Clin Endocrinol Metab* [Internet]. 2011 [cited 2023 May 14];96. Available
846 from: https://pubmed.ncbi.nlm.nih.gov/21289267/
847 36. Qiu T, Tian Y, Gao Y, Ma M, Li H, Liu X, Wu H, Zhang Y, Ding H, Cao M, Zhang J, Dai
848 J, Chen J, Cai H. PTEN loss regulates alveolar epithelial cell senescence in pulmonary
849 fibrosis depending on Akt activation. *Aging (Albany NY)* [Internet]. 2019 [cited 2023 Apr
850 19];11:7492. Available from: /pmc/articles/PMC6781970/
851 37. Bollong MJ, Yang B, Vergani N, Beyer BA, Chin EN, Zambaldo C, Wang D, Chatterjee
852 AK, Lairson LL, Schultz PG. Small molecule-mediated inhibition of myofibroblast
853 transdifferentiation for the treatment of fibrosis. *Proc Natl Acad Sci U S A*.
854 2017;114:4679–4684.
855 38. Schmid AC, Byrne RD, Vilar R, Woscholski R. Bisperoxovanadium compounds are
856 potent PTEN inhibitors. *FEBS Lett*. 2004;566:35–38.
857 39. Yang J, Yin Y. PTEN in Chromatin Remodeling. *Cold Spring Harb Perspect Med*
858 [Internet]. 2020 [cited 2023 Apr 18];10. Available from: /pmc/articles/PMC6996446/
859 40. Benitez JA, Ma J, D'Antonio M, Boyer A, Camargo MF, Zanca C, Kelly S, Khodadadi-
860 Jamayran A, Jameson NM, Andersen M, Miletic H, Saberi S, Frazer KA, Cavenee WK,
861 Furnari FB. PTEN regulates glioblastoma oncogenesis through chromatin-associated
862 complexes of DAXX and histone H3.3. *Nat Commun 2017 81* [Internet]. 2017 [cited 2024

863 May 16];8:1–15. Available from: https://www.nature.com/articles/ncomms15223
864 41. Shen WC, Lai YC, Li LH, Liao K, Lai HC, Kao SY, Wang J, Chuong CM, Hung SC.
865 Methylation and PTEN activation in dental pulp mesenchymal stem cells promotes
866 osteogenesis and reduces oncogenesis. *Nat Commun 2019 101* [Internet]. 2019 [cited 2024
867 May 16];10:1–13. Available from: https://www.nature.com/articles/s41467-019-10197-x
868 42. Yan F, Chen Z, Cui W. H3K9me2 regulation of BDNF expression via G9a partakes in the
869 progression of heart failure. *BMC Cardiovasc Disord* [Internet]. 2022 [cited 2024 May
870 16];22:1–13. Available from: https://link.springer.com/articles/10.1186/s12872-022-
871 02621-w
872 43. White ES, Atrasz RG, Hu B, Phan SH, Stambolic V, Mak TW, Hogaboam CM, Flaherty
873 KR, Martinez FJ, Kontos CD, Toews GB. Negative regulation of myofibroblast
874 differentiation by PTEN (phosphatase and tensin homolog deleted on chromosome 10).
875 *Am J Respir Crit Care Med*. 2006;173:112–121.
876 44. Geng J, Huang X, Li Y, Xu X, Li S, Jiang D, Liu Z, Dai H. Phosphatase and tensin
877 homolog deleted on chromosome 10 contributes to phenotype transformation of
878 fibroblasts in idiopathic pulmonary fibrosis via multiple pathways. *Exp Biol Med*
879 [Internet]. 2016 [cited 2023 Apr 27];241:157–165. Available from:
880 https://journals.sagepub.com/doi/10.1177/1535370215600100
881 45. Xie B, Zheng G, Li H, Yao X, Hong R, Li R, Yue W, Chen Y. Effects of the tumor
882 suppressor PTEN on the pathogenesis of idiopathic pulmonary fibrosis in Chinese
883 patients. *Mol Med Rep* [Internet]. 2016 [cited 2023 Apr 27];13:2715–2723. Available
884 from: http://www.spandidos-publications.com/10.3892/mmr.2016.4852/abstract
885 46. Nho RS, Hergert P. IPF Fibroblasts Are Desensitized to Type I Collagen Matrix-Induced
886 Cell Death by Suppressing Low Autophagy via Aberrant Akt/mTOR Kinases. *PLoS One*
887 [Internet]. 2014 [cited 2023 Apr 27];9:e94616. Available from:
888 https://journals.plos.org/plosone/article?id=10.1371/journal.pone.0094616
889 47. Im J, Hergert P, Nho RS. Reduced FoxO3a expression causes low autophagy in idiopathic
890 pulmonary fibrosis fibroblasts on collagen matrices. *Am J Physiol - Lung Cell Mol Physiol*
891 [Internet]. 2015 [cited 2023 Apr 27];309:L552–L561. Available from:
892 https://journals.physiology.org/doi/10.1152/ajplung.00079.2015
893 48. Mao P, Li J, Huang Y, Wu S, Pang X, He W, Liu X, Slutsky AS, Zhang H, Li Y.
894 MicroRNA-19b mediates lung epithelial-mesenchymal transition via phosphatidylinositol-
895 3,4,5-trisphosphate 3-phosphatase in response to mechanical stretch. *Am J Respir Cell Mol*
896 *Biol* [Internet]. 2017 [cited 2023 Apr 27];56:11–19. Available from: http://www.tm4.org/
897 49. Brito MB, Goulielmaki E, Papakonstanti EA. Focus on PTEN regulation. *Front Oncol*.
898 2015;5:166.
899 50. Kang YH, Lee HS, Kim WH. Promoter Methylation and Silencing of PTEN in Gastric
900 Carcinoma. *Lab Investig 2002 823* [Internet]. 2002 [cited 2023 Apr 24];82:285–291.
901 Available from: https://www.nature.com/articles/3780422
902 51. García JM, Silva J, Peña C, Garcia V, Rodriguez R, Cruz MA, Cantos B, Provencio M,
903 España P, Bonilla F. Promoter methylation of the PTEN gene is a common molecular
904 change in breast cancer. *Genes, Chromosom Cancer* [Internet]. 2004 [cited 2023 Apr
905 24];41:117–124. Available from: https://onlinelibrary-wiley-
906 com.colorado.idm.oclc.org/doi/full/10.1002/gcc.20062
907 52. Goel A, Arnold CN, Niedzwiecki D, Carethers JM, Dowell JM, Wasserman L, Compton
908 C, Mayer RJ, Bertagnolli MM, Boland CR. Frequent Inactivation of PTEN by Promoter

Hypermethylation in Microsatellite Instability-High Sporadic Colorectal Cancers. *Cancer Res* [Internet]. 2004 [cited 2023 Apr 24];64:3014–3021. Available from: https://aacrjournals.org/cancerres/article/64/9/3014/517889/Frequent-Inactivation-of-PTEN-by-Promoter

53. Mirmohammadsadegh A, Marini A, Nambiar S, Hassan M, Tannapfel A, Ruzicka T, Hengge UR. Epigenetic Silencing of the PTEN Gene in Melanoma. *Cancer Res* [Internet]. 2006 [cited 2023 Apr 24];66:6546–6552. Available from: https://aacrjournals.org/cancerres/article/66/13/6546/525928/Epigenetic-Silencing-of-the-PTEN-Gene-in-Melanoma

54. Xing XQ, Li B, Xu SL, Zhang CF, Liu J, Deng YS, Yang J. 5-Aza-2'-deoxycytidine, a DNA methylation inhibitor, attenuates hypoxic pulmonary hypertension via demethylation of the PTEN promoter. *Eur J Pharmacol* [Internet]. 2019 [cited 2023 Apr 24];855:227–234. Available from: https://pubmed.ncbi.nlm.nih.gov/31085236/

55. Nwachukwu N, Hagler M, Kafa R, Roos C, Miller J. Evidence for altered DNA methylation as a major regulator of gene expression in calcific aortic valve disease (671.15). *FASEB J*. 2014;28.

56. Gong L, Govan JM, Evans EB, Dai H, Wang E, Lee SW, Lin HK, Lazar AJ, Mills GB, Lin SY. Nuclear PTEN tumor-suppressor functions through maintaining heterochromatin structure. *Cell Cycle* [Internet]. 2015 [cited 2023 Feb 16];14:2323–2332. Available from: https://www.tandfonline.com/doi/abs/10.1080/15384101.2015.1044174

57. Horita H, Wysoczynski CL, Walker LA, Moulton KS, Li M, Ostriker A, Tucker R, McKinsey TA, Churchill MEA, Nemenoff RA, Weiser-Evans MCM. Nuclear PTEN functions as an essential regulator of SRF-dependent transcription to control smooth muscle differentiation. *Nat Commun* [Internet]. 2016 [cited 2023 Apr 19];7. Available from: /pmc/articles/PMC5411712/

58. Liu J-L, Sheng X, Hortobagyi ZK, Mao Z, Gallick GE, Yung WKA. Nuclear PTEN-Mediated Growth Suppression Is Independent of Akt Down-Regulation. *Mol Cell Biol* [Internet]. 2005 [cited 2023 May 11];25:6211. Available from: /pmc/articles/PMC1168816/

59. Walker CJ, Crocini C, Ramirez D, Killaars AR, Grim JC, Aguado BA, Clark K, Allen MA, Dowell RD, Leinwand LA, Anseth KS. Nuclear mechanosensing drives chromatin remodelling in persistently activated fibroblasts. *Nat Biomed Eng*. 2021;5:1485–1499.

60. Chen ZH, Zhu M, Yang J, Liang H, He J, He S, Wang P, Kang X, McNutt MA, Yin Y, Shen WH. PTEN Interacts with Histone H1 and Controls Chromatin Condensation. *Cell Rep* [Internet]. 2014 [cited 2023 Apr 25];8:2003. Available from: /pmc/articles/PMC4201947/

61. Jiang Y, Wang S, Zhao Y, Lin C, Zhong F, Jin L, He F, Wang H. Histone H3K9 demethylase JMJD1A modulates hepatic stellate cells activation and liver fibrosis by epigenetically regulating peroxisome proliferator-activated receptor γ. *FASEB J.* 2015;29:1830–1841.

62. Horita H, Wysoczynski CL, Walker LA, Moulton KS, Li M, Ostriker A, Tucker R, McKinsey TA, Churchill MEA, Nemenoff RA, Weiser-Evans MCM. Nuclear PTEN fucntions as an essential regularor of SRF-dependent transcription to control smooth muscle differentiation. *Nat Commun.* 2016;7.1;10830